

NACA TN 2559

4768



NATIONAL ADVISORY COMMITTEE FOR AERONAUTICS

TECHNICAL NOTE 2559

THEORETICAL AND EXPERIMENTAL INVESTIGATION OF
CONDENSATION OF AIR IN HYPERSONIC
WIND TUNNELS

By H. Guyford Stever and Kenneth C. Rathbun
Massachusetts Institute of Technology



Washington

November 1951

AFMTC
TECHNICAL LIBRARY
AFL 2811



TECHNICAL NOTE 2559

THEORETICAL AND EXPERIMENTAL INVESTIGATION OF
CONDENSATION OF AIR IN HYPERSONIC
WIND TUNNELS

By H. Guyford Stever and Kenneth C. Rathbun

SUMMARY

A theoretical and experimental investigation of the condensation of air in hypersonic wind tunnels has been carried out in the Aeronautical Engineering Department of the Massachusetts Institute of Technology. The experimental work was done with a hypersonic wind tunnel with a Mach number of approximately 7, located in the Gas Turbine Laboratory.

Condensation of air was detected and measured by condensation-fog light scattering, static-pressure measurements, and changes in wedge shock angles at degrees of supersaturation considerably lower than those predicted by existing condensation theory. The effects of varying supply pressures and temperatures were measured, and it was shown that preheating of the air so that it remained unsaturated or became only slightly supersaturated prevented the initiation of condensation.

The nucleation theory of condensation was modified to take account of a postulated variation of surface tension with decrease in size of the spontaneously formed drops which act as nuclei of condensation. Some such modification is shown to be necessary. The predicted condensation rates for a given degree of supersaturation are much higher than those predicted by the unmodified theory. The predicted condensation rates more nearly agree with the results of condensation measured experimentally on the assumption that condensation takes place on nuclei of oxygen and nitrogen.

Neither the theory modification nor the experimental measurements eliminate the possibility that the observed condensation takes place on nuclei of impurities such as water and carbon dioxide. However, the theory indicates that spontaneous condensation of oxygen and nitrogen can take place at relatively low amounts of supersaturation and that this will happen if condensation on foreign nuclei does not take place at even lower degrees of supersaturation.

INTRODUCTION

The expansion of air to high Mach numbers (5 or higher) in hypersonic wind tunnels lowers the temperature of the air well below the saturation temperature for oxygen and nitrogen, unless there is considerable preheating of the air before expansion, or unless the supply pressure is extremely low. Whether or not the supersaturated air condenses and at what values of pressure and temperature has been a matter for some investigation (references 1 to 9) in the past few years. The importance of exact information on the degree of supersaturation attainable is readily seen since such information makes it possible to determine the preheating temperature required in order to obtain condensation-free testing conditions in hypersonic-tunnel operation.

In the past, theoretical analyses of the condensation of the principal components of air have been confined to an analysis of the kinetics of condensation of pure nitrogen and pure oxygen. Some experimental evidence is now being interpreted as showing that oxygen and nitrogen condense on nuclei of impurities rather than on the self-generated nuclei postulated in the pure-vapor theory, and theoretical attacks are being made on this point. To be specific, condensation of air, which can be detected by light-scattering experiments and by detection of the discrepancies in the measured stream quantities of static and dynamic pressure, appears to start at only slight degrees of supersaturation, whereas the pure-vapor theories have predicted fairly substantial degrees of supersaturation before condensation starts (references 1 and 2).

The condensation of air in hypersonic tunnels is similar to two other much more widely investigated condensation phenomena, namely, the condensation of steam in steam nozzles and the condensation of water vapor in wind tunnels at high-subsonic and supersonic speeds. Head (reference 10) has a good bibliography on this subject. In the condensation of steam and of water vapor in air, Lukasiewicz (reference 11) summarized the results of a number of experimental investigations to show that about the same amount of adiabatic supercooling was present in both cases, about 47° to 63° C, with only a slight variation over a wide range of stagnation relative humidity of the water vapor and over a wide range of stagnation pressures and temperatures of the steam or humid air.

Both the steam condensation and the water vapor in air condensation are marked by a rapid growth of drops to a visible mist, as well as a sudden change in the gas flow conditions due to the sudden release of heat of condensation to the vapor. The so-called condensation shocks which result, while not shock waves in the true sense, cause rapid changes in the state of the gas in the stream and upset quantitative measurements. Experimental investigations of condensation of air in

hypersonic wind tunnels have used the same general techniques as have the water-vapor and steam nozzle investigations.

In the present investigation the theory of kinetics of condensation is analysed and some of its weaknesses are discussed. In particular, the theory is modified to take into account the dependence of surface tension on the radius of curvature of the drops onto which condensation is taking place. This modified condensation theory is applied to pure oxygen and nitrogen and its predictions are compared with those of the unmodified theory of condensation.

A hypersonic wind tunnel with an operating Mach number of about 7 has been designed, constructed, and used for experimental measurements of air condensation employing the light-scattering and schlieren technique, measurement of stream quantities, and measurement of the change in wedge shock-wave angles.

This work was conducted at the Massachusetts Institute of Technology under the sponsorship and with the financial assistance of the National Advisory Committee for Aeronautics.

SYMBOLS

The following symbols are used in this report:

N	number of molecules
N_l	number of molecules in liquid phase
N_v	number of molecules in vapor phase
U	evaporation energy
U_∞	evaporation energy of single molecule in an infinite extent of liquid
r	radius of liquid drop
r^*	radius of liquid drop of critical size
g	number of molecules in liquid drop
g^*	number of molecules in liquid drop of critical size
p	static pressure of vapor

p_{∞}	saturation vapor pressure in equilibrium with liquid surface of infinite radius of curvature
p_0, P_0	stagnation pressure of vapor
σ	surface tension of liquid
σ_{∞}	surface tension of flat liquid surface
w	surface energy per unit surface
W	surface energy
v_l	volume of liquid molecule
v_v	volume of vapor molecule
k	Boltzmann's constant, universal gas constant referred to one molecule
T	absolute temperature
T_0	stagnation absolute temperature
ϕ, Φ	thermodynamic potential
ϕ_v	thermodynamic potential of single vapor molecule
ϕ_l	thermodynamic potential of single liquid molecule
$\frac{1}{N} \frac{dN}{dt}$	fractional condensation rate
m	mass of molecule
d	density of liquid phase
S	entropy
D	intermolecular distance in liquid phase
ω, α, θ	angles in a geometrical construction in appendix A
ω	stream deflection angle behind oblique shock
α	oblique shock angle

ANALYSIS

Kinetics of Condensation of a Pure Vapor

In a wind tunnel or nozzle the vapor which has been expanded to a low temperature and pressure is not in contact with the solid walls, being insulated from them by the boundary layer. Hence, any condensation which takes place must be at an interface between the vapor and liquid nuclei spontaneously formed within the vapor or between the vapor and foreign nuclei, either solid or liquid. Thus, in one sense, the condensation problem for wind tunnels and nozzles is simplified since problems concerning the interface between the vapor and walls do not enter. Another feature of the condensation problem applied to rapidly expanding vapors is the shortness of time available for nuclei to form and to grow. This introduces as a most important element of the problem the kinetics of condensation. Both of these features of condensation have received considerable theoretical and experimental attention.

One of the most important and earliest contributions to condensation theory came when Thomson and Von Helmholtz (references 12 and 13) investigated the equilibrium vapor pressure for coexistence of both the vapor and a liquid drop of a substance, recognizing that the curvature of the interface was the determining factor in the problem. These analyses lead to the concept of the critical size drop.

The kinetic theory of condensation was primarily the contribution of Becker and Doring (reference 14) with contributions by Volmer (reference 15), Volmer and Weber (reference 16), Kaischew and Stranski (reference 17), Farkas (reference 18), and Zeldovich (reference 19). In this paper the slightly modified form of this theory presented by Frenkel (reference 20) will be followed. The next two subsections are a review of the work in references 12 to 19, treated to give an understanding of the condensation theory and as background for the modifications to the theory to be presented later.

Vapor pressure in equilibrium with a drop and critical-size-drop concept.- Considering a spherical drop with N_l liquid molecules and a radius r in contact with its vapor at a pressure p , the entire system being at a temperature T , the evaporation energy of the drop is equal to

$$U(N) = N_l U_\infty - 4\pi r^2 \sigma$$

where U_∞ is the evaporation energy of a large mass of the liquid referred to one molecule and σ is the surface tension. This

evaporation-energy expression represents the physical fact that the surface molecules of the drop are closer to the vapor state, energywise, than the internal molecules, by virtue of having fewer molecular bonds holding them in the liquid phase. The energy U_∞ is interpreted as that necessary to break all the molecular bonds holding an internal molecule of the drop.

The energy U_{N_l} required for the evaporation of one molecule from a drop of N_l molecules is

$$U_{N_l} = \frac{dU(N)}{dN_l} = U_\infty - 4\pi\sigma \frac{dr^2}{dN_l}$$

assuming as is usually done that the surface tension σ does not vary with size of drop. This assumption will be examined more thoroughly later.

The variable is changed from N_l to r by

$$\frac{4}{3} \pi r^3 = v_l N_l$$

$$4\pi r^2 dr = v_l dN_l$$

where v_l is the volume of a liquid molecule. Therefore

$$U_{N_l} = U_\infty - \frac{2\sigma}{r} v_l$$

Boltzmann's law shows that the vapor pressure around a drop consisting of N_l molecules is proportional to $e^{-U_{N_l}/kT}$. Therefore

$$p = p_{N_l} = \text{Constant} \times e^{-U_{N_l}/kT}$$

$$p_\infty = \text{Constant} \times e^{-U_\infty/kT}$$

Combining these,

$$\begin{aligned} \frac{p}{p_{\infty}} &= e^{-\left(U_{N_l} - U_{\infty}\right) / kT} \\ &= e^{2v_l \sigma / r kT} \end{aligned} \quad (1)$$

This formula derived by Thomson and Von Helmholtz expresses the relation, at a constant temperature T , between the equilibrium vapor pressure p and the radius r of the drop of liquid, in terms of p_{∞} , v_l , and σ all of which are properties of the substance and are dependent on the temperature, and k , a universal constant. Here p_{∞} is the vapor pressure in equilibrium with a drop of infinite radius, a flat surface of the liquid.

A physical argument shows that the equilibrium between vapor and liquid drop expressed by equation (1) is an unstable one. Consider a drop of radius r which is in contact with an infinite extent of vapor at pressure p . If one molecule of the vapor is added to the liquid drop, the drop radius increases while the vapor pressure of the infinite extent of vapor does not change. According to expression (1) the slightly enlarged drop has a lower equilibrium vapor pressure, so the existing vapor pressure is greater than the new equilibrium pressure. Hence, condensation of the vapor onto the drop will continue.

Similarly, if one molecule of the drop evaporates to the gas, the smaller drop which results requires a higher equilibrium vapor pressure than the existing one, hence evaporation continues.

Thus this unstable equilibrium expressed by equation (1) leads to the concept of critical size drop. For a vapor at a fixed temperature T , if the pressure p is higher than the saturation pressure $p_{\infty}(T)$, there exists a critical radius of liquid drop such that, if a drop is larger than the critical radius, it will continue to grow by condensation, and, if the drop is smaller than the critical radius, it will continue to shrink by evaporation.

Condensation rates for a pure vapor.— In the condensation of a pure vapor in the absence of any solid or liquid interfaces, condensation is assumed to take place on spontaneously formed liquid nuclei of the substance. In the statistical treatment of a vapor, even when the thermodynamical state of the vapor is such that the vapor is not super-saturated but is a stable unsaturated vapor, there is a distribution of

liquid drops in the system given by the Gibbs formula

$$N(r) = Ce^{-\Delta\phi(r)/kT}$$

where $N(r)$ is the number of drops of radius r , $\Delta\phi(r)$ is the energy of formation of such a drop given by the change in thermodynamic potential, and C is a constant which is equal to the sum of the molecules of the system if the total number of drops is very small compared with the total number of molecules in the system. Thus the number of drops of given radius decreases with radius for this distribution characterizing a stable vapor state.

This decrease of number of drops with an increase in the radius, of course, depends on $\Delta\phi(r)$'s being positive. The energy required to form a drop of radius r out of vapor molecules $\Delta\phi(r)$ is

$$\Delta\phi(r) = -(\phi_v - \phi_l)\frac{4\pi r^3}{3v_l} + 4\pi\sigma r^2$$

where ϕ_v is the thermodynamic potential of a single molecule in the vapor state and ϕ_l is the thermodynamic potential of a molecule in the liquid state. Both ϕ_v and ϕ_l are functions of pressure and temperature. This expression then contains two terms: The first is the difference in energy of a molecule in the liquid and gaseous states, multiplied by the number of molecules $\left(\frac{4\pi r^3}{3v_l}\right)$ in the drop, and the other is the surface energy term $4\pi\sigma r^2$. Since $\phi_l > \phi_v$ for the unsaturated state, the term $\Delta\phi(r)$ is always positive in the unsaturated state.

When, however, the vapor is in a state of supersaturation, the number of drops of given radius decreases with radius only up to the critical drop size, then it increases rapidly. This increase is due to the fact that $\Delta\phi(r)$ reaches a maximum at the critical drop size. This can be seen by noting that $\phi_l < \phi_v$ for any supersaturated state so that the term $\Delta\phi(r)$ has a negative and a positive term in it. Frenkel (reference 20) shows that $\Delta\phi(r)$ reaches a maximum at the critical radius as given by the Thomson formula (1). For larger values of drop radius, $\Delta\phi(r)$ decreases monotonically.

Hence the growth of a nuclei to the critical drop size is the crux of the condensation-rate problem, since it becomes a stable liquid drop and continues to grow thereafter. Once it has reached critical size it can be considered condensed. Actually all of these critical size drops continue to grow and their growth contributes to the rate of condensation. However, the rate of condensation of a vapor is primarily determined by the growth of nuclei to the critical size. It is the analysis of that problem that Becker and Doring and others (references 14 to 19) have carried out.

The results of these condensation-rate theories will be used here in the form presented by Frenkel (reference 20) without going through the analysis. There is one point in the derivation which should be mentioned, however. The growth of nuclei when there are but a few molecules present takes place in large discrete steps by the condensation or evaporation of a single molecule. This can be described by a difference equation. In the analysis the difference equation is changed to a differential equation and the growth or decay of the drop size is treated as a continuous phenomenon. Hence, the results do not apply to drops which include only a few molecules, and the results of this condensation-rate theory should not be applied much below a radius which is about 1.5 times the diameter of a molecule of the substance.

The rate of condensation of a pure vapor at pressure p and temperature T is¹

$$\frac{1}{N} \frac{dN}{dt} = e^{-\frac{4\pi\sigma(r^*)^2}{3kT}} \frac{p}{kT} \frac{4}{3} (r^*)^3 \sqrt{\frac{2\pi\sigma}{m}} \quad (2)$$

where r^* is the critical radius given by

$$r^* = \frac{2\sigma v_l}{kT \log_e p/p_\infty}$$

¹Frenkel's expression apparently has an insignificant error of π . This expression differs from the result obtained by Becker and Doring by a factor $(g^*)^{2/3}$, which is not very great in regions of high condensation rate.

and the other symbols are as follows:

$\frac{1}{N} \frac{dN}{dt}$	fractional rate of condensation
σ	surface tension (considered constant with respect to radius)
v_l	volume of a molecule of liquid phase
k	Boltzmann's constant
m	mass of a molecule (equals volume of molecule of liquid phase divided by density of liquid phase d)
d	density of liquid phase
p_∞	vapor pressure in equilibrium with flat surface

In this expression for the condensation rate the surface tension σ , the density d , the liquid molecular volume v_l , and the vapor pressure over a flat surface p_∞ are all considered to be functions of temperature only.

Condensation-rate theory applied to oxygen and nitrogen.- If the properties σ , v_l , p_∞ , and d are known as functions of T for a given vapor, it is possible to use the condensation-rate formula (2) to calculate rates for a given pressure and temperature; hence, a family of constant rate² lines can be plotted on a pressure-temperature plot for the vapor. This has been done by Head (reference 10) for water vapor in calculating the expected condensation of steam in steam nozzles and of water vapor in wind tunnels. Also Charyk, Lees, and Bogdonoff (references 1 and 2) have plotted this for nitrogen and oxygen. Generally, some of the properties of the vapor, v_l , σ , p_∞ , and d , have to be extrapolated from measured values to values at lower temperature, and considerable error can be introduced. Especially, those factors which

²Condensation rate is often expressed in terms of J , the rate of formation of nuclei of critical size per unit volume. The relationship between J and $\frac{1}{N} \frac{dN}{dt}$ is

$$\frac{1}{N} \frac{dN}{dt} = \frac{Jg^*}{n}$$

where n is the number of molecules per unit volume. Since n is usually in the range 10^{15} to 10^{20} and g^* is usually in the range from 10 to 100, J values are much larger than $\frac{1}{N} \frac{dN}{dt}$ values.

appear in the exponent of e must be known accurately in order to secure accurate condensation-rate prediction. The surface tension appears as a cube in the exponent and the molecular volume appears as a square (after $(r^*)^2$ is substituted). Inaccuracies in the prediction of condensation rate are often laid to the inaccuracies in the values of these properties, especially of the surface tension.

In addition to the inaccuracies introduced by the extrapolation of the quantities σ , v_l , p_{∞} , and d to low temperatures, there is another due to the fact that sometimes supersaturated vapor condenses into the liquid phase and sometimes into the solid. Apparently a region exists, at least for water vapor, wherein there is a mixture of ice and water drops in the condensed phase, the proportion of ice to water increasing with the degree of supersaturation at which condensation takes place (references 10 and 21).

The condensation rates for pure oxygen vapor and pure nitrogen vapor are plotted in figures 1 and 2. The values of the surface tension σ for oxygen and nitrogen are taken from reference 22. These are plotted in figures 3 and 4 and the extrapolation to lower temperatures is seen from these figures to be from 70° K. The values of the saturation pressure p_{∞} as a function of temperature T were obtained from references 23 to 26. These are plotted in figures 5 and 6. Here no extrapolation is involved.

The data for the density of oxygen and nitrogen in the liquid state are shown in figures 7 and 8. The extrapolation of these data is from 68° K. These data were obtained from reference 22.

Turning back again to figures 1 and 2 showing the condensation rates of 0, 10^{-3} , 1, 10^3 , and 10^6 per second, there is drawn for illustration a curve representing an isentropic expansion of the vapor from the initial conditions $p_0 = 100$ atmospheres and $T_0 = 293^{\circ}$ K for nitrogen, and the same for oxygen. On this isentrope are marked the Mach numbers which would be obtained if this isentropic expansion were carried out in a convergent-divergent nozzle. It is seen that the saturation line for nitrogen is reached at a Mach number of about 3.7. For oxygen the saturation line is reached at a Mach number of about 3.2. Further discussion of these results is postponed until the modification of the theory is developed.

The question arises as to what value of the condensation rate should be chosen as a criterion for condensation in a hypersonic wind tunnel. In the experiments reported herein the gas speeds are in the range from 2×10^3 to 3×10^3 feet per second and the tunnel is approximately 2 feet

long. Hence a rough figure for the time of condensation is 10^{-3} second. However, it will be noted from experimental evidence that the region of condensation occurring is shorter than the entire tunnel, so that 10^{-3} second is a maximum time. The other factor involved in selecting the criterion is the fraction of the vapor which must condense in order to affect appreciably the measurable stream quantities or to be detectable by a light-scattering experiment. In order to affect the stream quantities, an appreciable amount of latent heat must be released. In the most exhaustive experimental work to date on water-vapor condensation in wind tunnels, Head (reference 10) has calculated the nucleus formation rate J to be of the order of 10^{16} or higher in order to have sufficient heat released. When converted to fractional condensation rates, these turn out to be 10^2 per second or higher.

For the criterion for condensation of water vapor in air in supersonic tunnels of Mach number 1.45 and 2.0, it was concluded from unpublished experimental data obtained at the Lewis Flight Propulsion Laboratory of the NACA that a nuclei formation rate of about 3 to about 4×10^2 with an average of 50 was correct. In Head's work, these seemingly very low values of J are pointed out to be calculated using the unmodified theory, equation (2), which is believed to be considerably in error. As corrected by Head the theory shows that the experimental data correspond to J values of 10^{16} drops per cubic centimeter per second or higher.

Head also presents considerable evidence to prove a thesis that the criterion of condensation will vary with the rate of expansion of the vapor expressed in degrees temperature change per unit length along the nozzle. This latter factor is important in determining how close the gas is to a static state, since the condensation theory outlined earlier assumes certain equilibrium conditions. With respect to time delays encountered in the condensation process in wind tunnels, Kantrowitz (reference 27) has recently modified the Becker-Doring theory to take account of the time delay in the nucleation rate due to a statistical "random walk" phenomenon in the growth of the nuclei. That is, molecules may attach or detach from a growing nuclei, and the process of their growth must take into account both of these occurrences, with the net growth being the desired quantity.

Modification of Condensation Theory Due to Variations of Surface Tension with Surface Curvature

In experiments on condensation of steam in steam nozzles and water vapor in wind tunnels, the point at which the degree of supersaturation

reaches its maximum and condensation begins is clearly at a point where the critical size drops are very small, containing only a few molecules. This has long been recognized, and many writers on condensation theory and experiment have pointed out two ways in which this fact affects the theory of condensation. One of these enters the theory at the point where the basic difference equations, which can be written from considering the change in a droplet by either the condensation or the evaporation of a single molecule, are changed into differential equations and a continuous process is assumed. Thus caution must be exercised in the use of the Becker-Doring or similar rate theories in supersaturated regions where the critical drop sizes are of less than 10 or 12 molecules lest serious errors be introduced.

The other manner in which the small critical drop size introduces a problem is in its effect on the value of surface tension. It is quite clear, from a consideration of the number of molecular bonds holding a molecule to the surface of a small drop compared with the number holding it to the surface of a large drop, that the surface tension of a drop is dependent on the radius of the drop, noticeably so for small drops with only a few molecules in them.

To show for nitrogen the smallness of the size of the critical drops, figure 9 is plotted giving the condensation-rate lines for pure nitrogen on the Becker-Doring theory. An isentrope for the nitrogen in an expansion from a stagnation pressure of 100 atmospheres and a stagnation temperature of 293° K is shown as a dashed line. Across these curves are two broken lines indicating critical drop sizes of $1.5D$ and $2.5D$ where D is the diameter of a single molecule of nitrogen. A drop of radius $1.5D$ contains a dozen or so molecules and a drop of radius $2.5D$ contains 50 or 60 molecules. From figure 9 it is seen that, in the isentropic expansion of nitrogen, the number of the molecules in a critical drop is less than about a dozen by the time the fractional condensation rate has reached 1 per second, at a Mach number slightly greater than 5.

This dependence of surface tension on drop radius and its effect on condensation theory is the subject of investigation of this section. Two other published articles on condensation have considered this problem. Head (reference 10) employed a corrected value of the surface tension for water vapor as derived by Tolman (reference 28). In using this corrected value of surface tension, it was substituted directly into equations (1) and (2) for the critical drop radius and the condensation rate. It is believed that this will tend to correct the critical drop radius and the condensation-rate formula in the right direction but the magnitude of the correction, used in this way, will be wrong. Actually, equation (2) must be derived in a modified form if it is assumed that the surface tension is a function of the radius. This will be done presently.

Bogdonoff and Lees (reference 2) used the physical fact of reduction in surface tension in an entirely different way. In their preliminary experiments on air condensation, they interpreted the fact that there was no abrupt condensation shock present as evidence of no condensation, an interpretation now generally believed to be erroneous. In explaining this apparent lack of condensation at very high degrees of supersaturation, where the unmodified condensation rate predicted rapid condensation, they assumed that the reduced surface tension permitted the spontaneously grouped molecules to evaporate to the vapor state immediately without growth. This interpretation now seems to neglect completely the other facet of the problem which is that, with a reduced surface tension, groups of molecules form more readily into liquid drops from a collection of vapor molecules, because the energy of formation is less. This will be discussed more fully presently.

Modification of expression for vapor pressure in equilibrium with a drop and critical drop size.- To find a modified Thomson formula (equation (1)) the assumption is made that w , the surface energy per unit surface, is a function of the radius r :

$$w = \sigma_{\infty} f(r)$$

where $f(r)$ is dimensionless and has the value of 1 for large values of the radius and σ_{∞} is a constant, the value of the surface tension at large radii. The surface tension and surface energy per unit surface are equal at infinite radius.

Now consider a system of N_v molecules of the pure substance in the vapor phase and N_l molecules in the liquid phase. If the liquid drop has a radius r and surface energy per unit surface w , the thermodynamic potential of the system can be written

$$\Phi = N_v \phi_v + N_l \phi_l + 4\pi r^2 w$$

where ϕ_v is the thermodynamic potential of a single molecule in the vapor state and ϕ_l is the thermodynamic potential of a single molecule in the liquid state (i.e., in a liquid of infinite extent so the molecule binding energy is unaffected by the presence of a surface).

The thermodynamic equilibrium of this system of a liquid drop immersed in its own vapor is expressed by the variation of the thermodynamic potential being equal to zero

$$\delta\Phi = 0$$

The continuity equation, or equation expressing the constancy of total number of molecules in the system, is

$$N_v + N_l = \text{Constant}$$

These latter two equations lead to

$$\phi_l - \phi_v + 4\pi\sigma_\infty \frac{d}{dN_l} \left[r^2 f(r) \right] = 0$$

Let v_l be the volume of one molecule in the liquid state. Then

$$N_l = \frac{4\pi r^3}{3v_l}$$

and

$$dN_l = \frac{4\pi r^2 dr}{v_l}$$

Hence

$$\phi_l - \phi_v + \frac{\sigma_\infty v_l}{r^2} \frac{d}{dr} \left[r^2 f(r) \right] = 0$$

Differentiating this gives

$$d\phi_l - d\phi_v = -\sigma_\infty v_l d \left\{ \frac{1}{r^2} \frac{d}{dr} \left[r^2 f(r) \right] \right\}$$

In the limit when $r \rightarrow \infty$ the ordinary condition of equilibrium is $\phi_l = \phi_v$. If this condition is satisfied at a given temperature T ,

the equation above will be satisfied at the same temperature at a different pressure depending on r .

Recalling the definition³ of the thermodynamic potential,

$$\delta\phi = -S dT + V dp$$

where S is the entropy, it is seen that, for fixed temperature T ,

$$d\phi_v = v_v dp$$

and

$$d\phi_l = v_l dp$$

Hence

$$(v_v - v_l) dp = \sigma_{\infty} v_l d \left\{ \frac{1}{r^2} \frac{d}{dr} [r^2 f(r)] \right\}$$

The volume of a molecule in the liquid phase v_l can be neglected compared with the volume of a molecule in the vapor phase, and the perfect gas law $v_v = kT/p$ can be assumed. Here k is Boltzmann's constant or the gas constant for one molecule. These lead to the equation

$$kT \frac{dp}{p} = \sigma_{\infty} v_l d \left\{ \frac{1}{r^2} \frac{d}{dr} [r^2 f(r)] \right\}$$

³More completely

$$\delta\phi = -S dT + V dp - dW'$$

where dW' is the nonmechanical work done in the change of state.

Integrating

$$\log \frac{p}{p_\infty} = \frac{\sigma_\infty v_l}{kT} \frac{1}{r^2} \frac{d}{dr} [r^2 f(r)]$$

or

$$\frac{p}{p_\infty} = e^{\frac{\sigma_\infty v_l}{kT r^2} \frac{d}{dr} [r^2 f(r)]} \quad (3)$$

For the case of constant surface energy per unit surface, $f(r) = 1$, equation (3) becomes

$$\frac{p}{p_\infty} = e^{\frac{2\sigma_\infty v_l}{kT r}}$$

which is Thomson's equation.

This modified equation (3) will be reconsidered after the discussion of the form of the dependence of surface energy as a function of radius.

Modification of condensation-rate expression.- The assumption of a dependence of surface energy per unit surface on drop radius must also be taken into account in the derivation of the expression for condensation rate. This can be done without repeating the entire derivation of Becker and Doring, or similar ones. Referring to Frenkel (reference 19), there is the following expression for fractional condensation rate:

$$\frac{1}{N} \frac{dN}{dt} = g^* D(g^*) e^{-\Delta\phi(g^*)/kT} \sqrt{\frac{\gamma}{2\pi kT}} \quad (4)$$

Here g^* is the number of molecules in a critical size drop and $D(g^*)$ is given by

$$D(g^*) = 3^{2/3} (4\pi)^{1/3} v_l^{2/3} (g^*)^{2/3} \frac{p}{\sqrt{2\pi m kT}}$$

where v_l is the volume of a molecule in the liquid phase, m is the mass of a molecule, k is Boltzmann's constant, and T is the absolute temperature; $\Delta\Phi(g^*)$ is the change in thermodynamic potential in the system when g^* vapor molecules form a drop of radius r^* and is given by

$$\Delta\Phi(g^*) = -(\phi_v - \phi_l)g^* + 4\pi(r^*)^2w$$

where ϕ_v and ϕ_l are thermodynamic potentials of single molecules in the vapor and liquid phases, respectively.

The second derivative γ of this change of thermodynamic potential with respect to the number of molecules in a drop, all evaluated at g^* , is

$$\gamma = - \left\{ \frac{\partial^2}{\partial g^2} [\Delta\Phi(g)] \right\}_{g^*}$$

With these expressions, account can be taken of the radius dependence of the surface energy per unit surface

$$w = \sigma_\infty f(r)$$

First it is necessary to find the proper expression for $\Delta\Phi(g^*)$.

$$\Delta\Phi(g) = -(\phi_v - \phi_l)g + 4\pi r^2 w$$

To evaluate $\phi_v - \phi_l$ at g^* it is recalled that in Frenkel's paper $\Delta\phi(g)$ has a maximum at $g = g^*$. Hence by differentiation

$$\begin{aligned}
 -(\phi_v - \phi_l)_{g^*} + \left[\frac{\partial(4\pi r^2 w)}{\partial g} \right]_{g^*} &= 0 \\
 (\phi_v - \phi_l)_{g^*} &= \left[\frac{\partial(4\pi r^2 w)}{\partial g} \right]_{g^*} = \left[\frac{v_l}{4\pi r^2} \frac{\partial(4\pi r^2 w)}{\partial r} \right]_{r^*} \\
 &= \left\{ \frac{v_l \sigma_\infty}{r^2} \frac{\partial}{\partial r} [r^2 f(r)] \right\}_{r^*}
 \end{aligned}$$

This leads to the expression for $\Delta\phi(g^*)$

$$\Delta\phi(g^*) = \left\{ -g \frac{v_l \sigma_\infty}{r^2} \frac{\partial}{\partial r} [r^2 f(r)] + 4\pi \sigma_\infty r^2 f(r) \right\}_{r^*}$$

Next an expression is obtained for γ .

$$\gamma = - \left\{ \frac{\partial^2}{\partial g^2} [\Delta\phi(g)] \right\}_{g^*}$$

Since $\Delta\phi(g) = (\phi_v - \phi_l)g + 4\pi r^2 w$

$$\gamma = - \frac{\partial^2(4\pi r^2 w)}{\partial g^2}$$

$$g = \frac{4\pi r^3}{3v_l}$$

$$dg = \frac{4\pi r^2 dr}{v_l}$$

$$\frac{\partial}{\partial g} = \frac{v_l}{4\pi r^2} \frac{\partial}{\partial r}$$

$$\frac{\partial}{\partial g}(4\pi r^2 w) = \frac{v_l \sigma_\infty}{r^2} \frac{\partial}{\partial r} [r^2 f(r)]$$

$$\frac{\partial^2}{\partial g^2}(4\pi r^2 w) = \frac{v_l^2 \sigma_\infty}{4\pi r^2} \left\{ \frac{1}{r^2} \frac{\partial^2}{\partial r^2} [r^2 f(r)] - \frac{2}{r^3} \frac{\partial}{\partial r} [r^2 f(r)] \right\}$$

All of these terms can now be collected into the expression for the fractional condensation rate with the dependence of the surface energy on drop radius included.

$$\frac{1}{N} \frac{dN}{dt} = \frac{(4\pi)^2}{3v_l} \frac{r_p^5}{\sqrt{2\pi mkT}} \sqrt{\frac{v_l^2 \sigma_\infty}{8\pi r^2 kT}} \left\{ \frac{2}{r^3} \frac{\partial}{\partial r} [r^2 f(r)] - \frac{1}{r^2} \frac{\partial^2}{\partial r^2} [r^2 f(r)] \right\} e^{\frac{-4\pi \sigma_\infty r}{kT}} \left\{ rf(r) - \frac{1}{3} \frac{\partial}{\partial r} [r^2 f(r)] \right\} \quad (5)$$

Equation (5) is evaluated for a value of r^* , the critical drop radius given by the modified Thomson formula (3).

When $f(r)$ is set equal to unity expression (5) reduces to expression (2) as it should.

Simplifying equation (5) and replacing partial derivatives by total derivatives, the following expression is obtained:

$$\frac{1}{N} \frac{dN}{dt} = \frac{4r^3 p}{3 kT} \sqrt{\frac{\pi \sigma_{\infty}}{m}} \sqrt{\frac{2}{r} \frac{d}{dr} [r^2 f(r)] - \frac{d^2}{dr^2} [r^2 f(r)]} e^{-\frac{4\pi \sigma_{\infty} r}{kT}} \left\{ r f(r) - \frac{1}{3} \frac{d}{dr} [r^2 f(r)] \right\} \quad (5a)$$

It is of interest to rewrite equations (3) and (5a) in terms of the surface tension σ which is also a function of the radius of curvature of the surface

$$\sigma = \sigma_{\infty} h(r)$$

To get the relationship between σ and w the equation for the surface energy W is used

$$W = 4\pi r^2 w = \int_0^A \sigma \, dA$$

where A is the surface of a drop of radius r .

$$\begin{aligned} w &= \frac{1}{4\pi r^2} \int_0^r \sigma 8\pi r \, dr \\ &= \sigma_{\infty} f(r) = \frac{2\sigma_{\infty}}{r^2} \int_0^r r h(r) \, dr \end{aligned}$$

or

$$f(r) = \frac{2}{r^2} \int_0^r r h(r) \, dr$$

This can be substituted into equation (3) yielding

$$\begin{aligned} \log \frac{p}{p_{\infty}} &= \frac{2\sigma_{\infty} h(r) v_l}{kTr} \\ &= \frac{2\sigma v_l}{kTr} \end{aligned} \quad (3a)$$

Hence, in terms of the radius-dependent surface tension, the Thomson equation (1) is unchanged in form.

The expression for $f(r)$ can also be substituted in equation (5a) for the fractional condensation rate, yielding

$$\frac{1}{N} \frac{dN}{dt} = \frac{4}{3} r^3 \frac{p}{kT} \sqrt{\frac{2\pi\sigma_{\infty}}{m}} \sqrt{h(r) - r \frac{d}{dr} [h(r)]} e^{\frac{-8\pi\sigma_{\infty}}{kT} \left[\int_0^r r h(r) dr - \frac{1}{3} r^2 h(r) \right]}$$

or

$$\frac{1}{N} \frac{dN}{dt} = \frac{4}{3} r^3 \frac{p}{kT} \sqrt{\frac{2\pi}{m}} \sqrt{\sigma - r \frac{d\sigma}{dr}} e^{\frac{-8\pi}{kT} \left(\int_0^r r \sigma dr - \frac{1}{3} r^2 \sigma \right)} \quad (5b)$$

If the variation with radius of either surface energy per unit surface or surface tension is known, it is possible to use either equation (5a) or (5b) to calculate modified condensation rates.

Dependence of surface tension on radius. - The surface energy of a drop is

$$W = 4\pi r^2 w = 8\pi \int_0^r \sigma r dr$$

The factor r^2 in this expression for the surface energy led Thomson and Von Helmholtz to the conclusion that the vapor pressure in equilibrium with a curved liquid surface is greater than that in equilibrium with a flat surface. This leads to the concept of the critical drop

size and to the kinetic theory of condensation. In the preceding sections it has been shown that the usually employed expressions for the critical drop size and condensation rate must be modified if the variation of surface tension with radius of curvature is to be taken into account. The form of the assumed variation was

$$\sigma = \sigma_{\infty} h(r)$$

The form of the function $h(r)$ has been a matter discussed by many since the time of Thomson's (reference 12) early work in this field. There is always a question remaining concerning the accuracy of any expression derived on macroscopic thermodynamic principles because, at the very small radii of curvature of interest in condensation theory, the drops are made up of only a small number of molecules where continuum concepts are not valid. Attempts have been made (e.g., by Mayer and Mayer (reference 29)) to carry out a condensation analysis for a perfect gas on statistical mechanical principles. Again, the problem of calculating the energy of a cluster of molecules forming a small drop, in order to calculate the distribution of drop sizes, comes into the analysis. The energy of formation of drops of a very small number of molecules (2, 3, 4) can be calculated, but the calculations become extremely complex as one goes to higher and higher numbers of molecules. One is left then with the situation that statistical mechanical treatment of the problem from the low end and thermodynamical macroscopic treatments from the high end of the drop radius are both weak in the region of 10 to 100 molecules, a very important region for condensation theory.

Recently, Tolman (reference 28) developed a quasi-thermodynamic form of the variation of surface tension with radius. This has been qualitatively verified by a statistical mechanical treatment by Kirkwood and Buff (reference 30). Tolman's simplified expression for the surface tension is

$$\sigma = \sigma_{\infty} \frac{1}{1 + \frac{2\delta}{r}} \quad (6)$$

where δ is almost a constant for a given substance and ranges from about 0.25 to 0.6, the intermolecular distance in the liquid state.

Steyer (reference 31) described a simple physical picture of the dependence of surface energy per unit surface on radius and from this

developed a formula for this dependence. This analysis used the physical concept that the surface tension of a drop is due to molecular bonds for molecules on the surface being fewer in number than for those in the interior of the drop. To calculate accurately the binding energy of a surface molecule would require calculating the energy of every bond between the surface molecule and all other molecules. However, the intermolecular forces die off rapidly with distance, and a good approximation to the binding energy of a surface molecule can be found by considering only bonds to nearest neighbors. Figure 10 illustrates for spherical molecules how the number of closest neighbors decreases as the radius of curvature of the surface decreases. A simple calculation involving the solid angle, intercepted at a surface molecule, of all its closest neighbors then gives an approximate variation of surface energy per unit surface with radius. This calculation is carried out in appendix A. The resulting formula for surface energy per unit surface is

$$w = \sigma_{\infty} \frac{2}{3} \left(1 + \frac{\sqrt{r^2 - rD}}{2r - D} - \frac{\sqrt{3}}{2} \frac{D}{2r - D} \right) \quad (7)$$

Application of modified condensation theory to pure-vapor condensation.- The modified theory developed above is now applied to the condensation of pure nitrogen and pure oxygen. Tolman's expression (6) for the surface tension is used with a value of $\delta = \frac{1}{2}D$

where D is the intermolecular distance. Figure 11 is a plot of condensation rate lines on a pressure-temperature graph for oxygen and figure 12 is a similar one for nitrogen. Again an isentropic expansion is plotted as a dashed line crossing the rate lines, in this case for a stagnation pressure of 100 atmospheres and a stagnation temperature of 293° K. Also a broken dashed curve is shown for a critical size drop of radius $r = 1.5D$.

If one is dealing with a pure-nitrogen expansion, or if air acts like pure nitrogen, it is seen from figure 12 that the nitrogen or air would expand from 100 atmospheres to slightly below 1 atmosphere where it would enter the supersaturated region at a Mach number of about 3.7. When the expansion had reached $M = 4.3$ the fractional condensation rate would be very high, about 10^6 per second. For oxygen, or if air acts like oxygen, from figure 11 it is seen that supersaturation is reached near $M = 3.1$ and a rate of 10^6 per second is reached at $M = 3.6$.

Comparing figures 11 and 12 with figures 1 and 2, respectively, it is clearly seen that the modification of the theory due to surface-tension variation with curvature changes the predicted condensation rates so that the condensation rates are much higher for a given degree of supersaturation and condensation takes place much closer to the saturation line than in the unmodified theory. This conclusion is directly opposite from that of Bogdonoff and Lees (reference 2) and also opposite from the original interpretation which the author (reference 31) put on the correction to the theory which a varying surface tension would make.

Because of the fairly close crowding of the lines of high rates of condensation to the saturation lines, in figures 11 and 12, one would not expect to obtain very high degrees of supersaturation of either pure oxygen or nitrogen, or of air which probably acts in some manner averaged between the behavior of nitrogen and oxygen. It is seen that high rates are reached before the critical radius has dropped below a value of 1.5D, or, in other words, before the drops get below 10 or 12 molecules in size.

A further discussion of these points will be made in this report after the results of experiments are presented.

DESCRIPTION OF APPARATUS

The apparatus which has been used in the experimental investigations of the condensation of air at high Mach numbers is a hypersonic wind tunnel located in the Gas Turbine Laboratory at the Massachusetts Institute of Technology. This tunnel is of the blowdown type with a design Mach number of 7.2. The test section has a cross section of 2.25 inches by 2.75 inches. Both supply pressure and supply temperature are held constant during a run, although it is possible to vary both of these from run to run and to vary the pressure during a run. The range of supply temperature is from 530° R to 1300° R. The range of supply pressure is from about 300 pounds per square inch absolute to 3000 pounds per square inch absolute, but the runs become impractically short at the high end of the pressure range. At pressures lower than 300 pounds per square inch absolute the flow in the tunnel is subsonic through part of the nozzle.

General Arrangement of Equipment

A schematic diagram of the arrangement of all of the principal and auxiliary equipment is shown in figure 13. In the charging operation, atmospheric air is taken into the system through a large, activated-alumina dryer. The air is compressed to 3000 pounds per square inch

absolute in the compressor and passes through a dryer designed to remove oil and water impurities by cooling. It passes then through a filter which removes small entrained particles of water, oil, or other impurities and enters the storage bottles.

During a run, the stored compressed air is discharged through a pressure-regulating valve into the heat-storage unit. The air emerges at constant temperature and pressure and passes through a small settling chamber before entering the nozzle. Following the nozzle and test chamber are two diffuser sections which lead into a pipe to a steam ejector.

Nozzle

The nozzle and test-section blocks are shown in figure 14, both separately and partially assembled. The supersonic portion of this nozzle was designed by the method of characteristics following Busemann (reference 32) and with the assumptions that the gas obeyed the perfect-gas law and had a constant ratio of specific heats of 1.4. Neither of these assumptions is entirely valid but the error introduced by them has been estimated to be small. An allowance for boundary-layer growth was made, which agrees fairly well with the results observed in schlieren photographs of the flow.

The subsonic portion of each nozzle block is a quarter arc of a circle of $1\frac{1}{8}$ -inch radius. The blocks are steel, $2\frac{1}{4}$ inches wide and 24 inches long. When the nozzle blocks are assembled in the metal frame, the nozzle throat is a slit 0.019 inch by $2\frac{1}{4}$ inches and the test section is $2\frac{1}{4}$ inches by $2\frac{3}{4}$ inches in cross section. The expansion takes place in the first 8.67 inches of the nozzle, approximately constant Mach number being attained in the last 15 inches. There is a continued divergence of the blocks to a final $2\frac{7}{8}$ inches.

Pyrex glass windows $\frac{3}{4}$ inch thick are used for the transparent walls of the nozzle and test section. These windows extend right up to the throat where the pressure is quite high. Tests have been run at temperatures up to 1090° R and pressures up to 2700 pounds per square inch absolute without failure of these windows, although serious break-age trouble was encountered with non-heat-resistant glass and glass of less thickness mounted somewhat differently. A continuous $\frac{1}{8}$ -inch silicone rubber gasket is used to seal the glass walls. Eighteen static-pressure taps 0.020-inch diameter on 1-inch centers are provided on one

of the nozzle blocks, starting at a station where the design Mach number is 5.9.

Diffuser

The diffuser is made in two sections. The first is a straight section of square tubing, $2\frac{1}{4}$ inches by $2\frac{1}{4}$ inches inside and about 2 feet long. The second is a diverging piece of square cross section, 18 inches long, diverging from $2\frac{1}{4}$ inches by $2\frac{1}{4}$ inches to 5 inches by 5 inches. These two sections can be seen in figure 15. A converging entrance or second throat is formed in a block just ahead of the first section of the diffuser, the end of the nozzle test section having inside dimensions of $2\frac{1}{4}$ inches by $2\frac{7}{8}$ inches. The purpose of the straight length is to allow the air, after separation from the wall following the shocks, to reattach to the wall before entering the subsonic diffuser. This design incorporates some of the features suggested by Neumann and Lustwerk (reference 33).

Temperature Regulation and Heater

The heater consists of a section of high-pressure pipe in which aluminum rods are placed, the pipe being fitted with electrical heating units and enclosed in a large box containing insulation. The pipe, minus box, insulation, and electrical heaters, is shown in figure 16. It has an $8\frac{1}{2}$ -inch inside diameter with a $1\frac{1}{8}$ -inch wall and is about 17 feet long. This pipe is loaded with 1000 pounds of 1/16-inch-diameter aluminum wires as shown in figure 17. The wires are placed inside the pipe in 16 bundles, each 12 inches long, separated from each other by 28-mesh stainless-steel screens. The purpose of the screens separating the bundles is to retard the flow of heat longitudinally along the wires. An air distribution baffle precedes the first bundle, and a spacer follows the last to prevent the wires from being displaced and to allow for mixing of the air from the many flow channels. The pipe is heated by means of 39 strip heaters, 1250 watts each, giving a total capacity of about 49 kilowatts. The pipe, flanges, and heating strips are enclosed in a plywood box, 30 inches by 30 inches by 19 feet long, in which vermiculite insulation is packed. The top panels of the box, just over the two flanges, are made of asbestos sheet instead of plywood. The completed heater is shown in figure 16(a).

During the course of a run the incoming air cools the aluminum wires progressively down the pipe. Since much more heat is stored in the aluminum wire than is used to heat the air used in a run, only the first sections of wire are cooled appreciably, the temperature of the final sections of the heat exchanger being practically unchanged. The open area, that is, the space between the wires through which the air passes, is about 9 percent of the inside area of the pipe, or roughly the equivalent of a $2\frac{1}{2}$ -inch standard pipe. The flow is turbulent for all conditions under which the tunnel is operated, and calculations predict a surface heat-transfer coefficient of about 96 to 126 Btu per hour per square foot per °F. The small passageways are chiefly responsible for this high coefficient. The amount of surface area available for heat transfer is about 5100 square feet. Pressure drop through the heat exchanger is negligible (2 to 10 lb/sq in.) considering the available pressure of 3000 pounds per square inch absolute.

The stagnation temperature in the stilling chamber in front of the nozzle is measured by a Chromel-constantan thermocouple which protrudes into the middle of the air stream. Thermocouples are also attached to the outside surfaces of the heater, to monitor the heater temperature during the heating period. It is found that a complete discharge of 500 pounds of air can be made without appreciable changes in stagnation temperature. During the course of a day the heater cools about 100° R with the initial temperature at 1000° R, so the reheating problem is not very great.

Compressor, Dryers, and Air-Storage Bottles

Air at 3000 pounds per square inch absolute is supplied by a four-stage Ingersoll-Rand water-cooled compressor which is shown in figure 18. The air intake to the compressor is connected to an activated-alumina drying unit. The compressor capacity is 70 cubic feet per minute of free air. The back pressure is kept at 3000 pounds per square inch absolute in order to increase the water vapor separation in the aftercooler. The compressor is equipped with intercoolers and an aftercooler so that the air leaves at about room temperature. From the compressor, the air passes through another dryer and purifier, which is a specially designed heat exchanger containing a coolant mixture of dry ice and alcohol at a temperature of about 365° R. This unit is shown in figure 18. From the dryer it passes through a filter to separate solid or liquid particles down to a diameter of 3 microns. Air leaving this dryer has a measured dew point of 430° R or lower.

The dry air is stored in 11 bottles or flasks, which are shown in figure 19, having a total capacity of 34 cubic feet, holding roughly

500 pounds of air at 3000 pounds per square inch absolute. After pumping up the bottles, a valve located between them and the dryer is closed to isolate the charging equipment from the discharging equipment. Approximately $1\frac{1}{2}$ hours are required for loading the flasks.

Pressure Regulation and Instrumentation

The pressure in the stilling section in front of the nozzle, which is the initial stagnation pressure of the nozzle, is controlled by a commercially available, pressure-loaded dome and diaphragm-type regulating valve which steps down the pressure of the air stored in the bottles to the desired operating pressure. The valve can be seen in figure 16. The diaphragm loading air is not taken directly from the stilling section but is from a secondary supply of approximately 100 pounds per square inch absolute reduced to 35 pounds per square inch absolute. Pressure variations in the stilling section are converted to pressure variations of this secondary air supply by means of a commercially available pressure controller, and, in turn, the secondary air supply regulates the opening of the valve. A simple dial-setting operation serves to select the pressure in the stilling section which can be varied from 0 to approximately 3000 pounds per square inch absolute, the full storage-bottle pressure. The instrument system does not control so well as expected so it is necessary to reset the dial manually continuously throughout a run. Pressure control within approximately 2 percent is achievable this way. The pressure variations of 2 percent are relatively slow, so that it was found possible, by careful timing, to take schlieren, light-scattering, and static-pressure pictures at a value of stagnation pressure within 1 percent of the desired pressure.

The static wall pressures on the tunnel and diffuser walls are measured by mercury manometers. A series of pictures of the manometer board is shown in figure 20. Since the pressures involved are generally higher than those used in most hypersonic tunnels, there is no serious static-pressure measuring problem. The manometer pressures can be read quickly and with reasonable accuracy from the manometers. The stilling-section pressure, which is considered the initial stagnation pressure, is measured on a 12-inch gage of Bourdon tube construction.

A five-pronged pressure rake is used to measure total head. This can be located at any place in the test section and nozzle, although its position is not changeable while air is flowing.

TEST PROCEDURE

Operation of Tunnel

In the charging period the only unusual feature is the operation of the cooling type of oil and water separator. This requires charging with the alcohol and dry-ice mixture for about a half hour before the air bottle charging starts, in order to cool the separator down to 365° R. The rest of the charging is a straightforward pumping operation requiring about $1\frac{1}{2}$ hours if the bottles are empty at the start of the operation.

Before a run is made, the heater is heated to operating temperature. This requires several hours if the amount of temperature rise is large. After the heater is brought up to temperature, the pipe leading to the stilling chamber, the stilling chamber, and the nozzle blocks and test chamber are all heated by allowing a slow bleed of air through the heater for about a half hour. The compressor is run continuously during this preliminary phase of operation in order to keep the supply pressure at 3000 pounds per square inch absolute.

When preparations for the run are complete, the steam ejector is turned on, bringing the pressure in the test chamber, diffuser nozzle, stilling chamber, and heater to about 1.5 pounds per square inch absolute. The pressure-control dial is then turned, opening the pressure-regulating valve and raising the pressure in the system. As the flow increases, the low pressure of the steam ejector increases somewhat. The tunnel establishes fully hypersonic flow when the stilling-chamber pressure is about 300 pounds per square inch absolute and the outlet pressure is about 3 pounds per square inch absolute giving a starting pressure ratio of 100. The pressure-control dial is then turned up so that the stagnation pressure is slightly above the pressure desired for the run. The pressure falls off slowly except as corrected by the manual operation of the control dial. The manual operation permits pressure regulation to within 1 percent of the desired value over the full hypersonic operating range from 300 pounds per square inch absolute to 3000 pounds per square inch. The possible lengths of run vary with pressure and temperature with typical figures of about 12 minutes at the lowest operating pressure, 300 pounds per square inch absolute and room temperature and 4 minutes at 1000 pounds per square inch absolute and room temperature.

Condensation Experiments

The condensation tests involved measurement of static and stagnation pressures and stagnation temperatures. The methods of measurement

of these were described in the section "Description of Apparatus." They also involved schlieren photography of the flow in the tunnel and condensation light-scattering photography.

The schlieren photographs are made using a 5-inch-diameter, parallel-beam, schlieren system. Pictures are taken with the knife edge vertical. (Recall that the tunnel axis is also vertical.) The schlieren source is a high-pressure mercury-arc lamp which may be used as a steady source for observing the air-flow pattern on a ground-glass screen, or as spark source for photography with a duration of 5 to 10 microseconds. In order to take a complete schlieren pattern for the major part of the 24-inch nozzle and test section, seven overlapping pictures are taken, each on a separate run, with conditions duplicated, and these photographs are pieced together as in figure 21.

Photographs of the condensation fog are made by use of the optical equipment shown in figure 15. This equipment consists of a mercury-arc lamp, the light of which is made parallel by a condensing lens, after which it passes through a small hole in an opaque disk. The beam of light is shone through the transparent sidewalls of the tunnel, whereupon a small light spot appears on each window owing to light scattering from imperfections and scratches. (One of these spots may be seen in fig. 15.) By aiming the camera diagonally across the axis of the light beam either from above or below, a photograph showing both sidewall spots may be made. With proper camera angle, the space between the spots also can be arranged in the photograph appearing as a dark void. Reflections from the nozzle blocks sometimes appear, but these are never in the direct line between the spots. They are of no consequence. Close to the throat of the nozzle the light beam must necessarily be of smaller diameter in order not to cover too much area.

A light-scattering photograph of the type shown in figure 22 is made by running at constant pressure long enough for a time-exposure photograph to be made. Condensation fog (if any) scatters the light within the tunnel so that an image can be picked up by a photographic plate. All runs during which condensation scattering pictures are to be made are made at night in almost total darkness. The fog is sometimes visible. In condensation photographs using commercial film, 10 pounds of air are usually passed during the exposure, whereas for Plus-X negatives (higher Weston rating than commercial film) only 5 pounds of air flow are used. When the light beam is very small, as in figure 23, exposures are necessarily longer.

EXPERIMENTAL RESULTS

Condensation Light Scattering

Photographs of the light scattering from condensation fog are shown in figures 22 to 26. These photographs were taken, as described in the section "Test Procedure," with the optical axis of the camera at about 45° from the axis of the light beam. In figures 22 to 25 there are included some photographs taken when there was no flow, some for subsonic flow without condensation, and some for hypersonic flow without condensation. These have the characteristic two spots of light which is scattered from the two glass sidewalls of the tunnel. When condensation is present, as it is in many other pictures, the region of the photograph between these two spots is filled in. The intensity of the exposure gives a qualitative measure of the amount of condensation.

In figure 22, pictures 14, 15, 16, and 17 were taken to show intense condensation in several stations of the test section for an initial stagnation pressure of 1015 pounds per square inch absolute and a stagnation temperature of 530° R. Picture 7 is a reference picture taken when there was no air flow to show the light scattering from the two window spots. These pictures were taken with a light beam of about $1\frac{3}{4}$ inch diameter.

In order to take condensation pictures farther into the throat the light beam was reduced in size to about $\frac{3}{4}$ inch and the pictures shown in figure 24 were taken. Here pictures 21, 22, and 24 show condensation-fog light scattering at three stations in the nozzle with Mach number varying from 4.9 to 5.4 in picture 21, from 5.6 to 6.0 in picture 22, and from 6.1 to 6.3 in picture 24. These pictures were taken at an initial stagnation pressure of 1015 pounds per square inch absolute and an initial stagnation temperature of 530° R. These three pictures should be compared with picture 18 which had the same time exposure with no flow, showing the two spots of scattered light from the windows, as well as two reflections from the nozzle blocks and some reflections from the metal plate which holds the nearer glass window in place. Pictures 19 and 20 were taken with longer exposures, 19 where there was no flow and 20 when the flow was subsonic. For the subsonic case there is no condensation fog visible, even though the amount of air which passed through the tunnel during the 2-minute exposure was the same as the amount which flowed in pictures 21, 22, and 24.

The dependence of the amount of condensation on the initial stagnation pressure is shown in figure 25. Here a comparison of pictures 9, 10, and 11, taken at initial stagnation pressures of 338, 508, and 1015 pounds per square inch absolute, respectively, shows distinctly

the increase of the condensation fog with increase in pressure. All of these pictures were taken at an initial stagnation temperature of 530° R and with a total of 10 pounds of air flowing during the exposure. A comparison picture, 8, is also shown in figure 25 which shows no condensation fog visible for a total of 12.7 pounds of air flowing at a subsonic speed. Because of the much longer exposure there is more scattered light generally in picture 8, but there is no fog scattering between the two window spots.

In order to test how close to the nozzle throat condensation fog could be detected, the series of pictures shown in figure 23 was taken. The nature of these pictures apparently is different although the same light-scattering technique was used. First, the parallel light beam was reduced in diameter to about $1/8$ inch. One of the window scattering spots of this $1/8$ -inch beam is seen in the upper center of each of the five pictures of figure 23. The pictures are all cut off just above where the other window scattering spot would have appeared in the lower center region. Reflections of the upper-window scattering spot are seen in the pictures, these reflections being from the curved highly polished nozzle blocks. From that it can be seen that the photograph is taken with the camera pointing down into the nozzle throat.

Pictures 32 and 34, taken where the Mach number ranges are 4.5 to 4.6 and 4.3 to 4.5, respectively, show a faint vertical bar of condensation-fog light scattering, the bar stretching from the window scattering spot down the center of the picture. These pictures can be compared with picture 33 taken with no flow at the same location for the same exposure duration of 80 seconds. Pictures 35 and 36 are similar photographs taken even closer to the throat where the Mach number ranges are 3.9 to 4.3 and 3.7 to 3.9, respectively, and there is no light scattering visible.

The effect of both stagnation temperature and stagnation pressure on condensation is shown in figure 26. The upper three pictures, 71, 69, and 61, are taken at room temperature at three different pressures, showing the increase in condensation with pressure. The lower three pictures, 57, 47, and 55, are taken at the higher temperatures 980° , 990° , and 1000° R, respectively, and with the same range of pressures as the upper three, namely, 338, 508, and 1015 pounds per square inch absolute. There is no condensation fog visible at the higher temperatures.

The Mach numbers given here are computed from the area ratios, assuming isentropic expansion. The design test-section Mach number is 7.2. Since static-pressure measurements indicate a test-section Mach number of 6.8, as pointed out in the next discussion, a correction factor of $6.8/7.2$ is applied. The design formula, originally allowing

for boundary-layer build-up, is thereby corrected to agree with experimental data. The formula is

$$M = \frac{6.8}{7.2} \left[1 + 6.2 \left(\frac{x}{8.67} \right)^{0.182} \right]$$

where M is the Mach number and x is the distance from the throat in inches.

Although the numbers thus calculated are presumably somewhat in error, no entirely satisfactory method for determining Mach number is available. The use of a wedge in the diverging section of the nozzle is impractical owing to excessive length and consequent vibration of the supporting arm. For the same reason, total-head measurements are also impractical in the diverging section.

Static-Pressure Measurements

In figure 27, there are plotted some typical static-pressure measurements along the nozzle and test section. Data are plotted for six runs, and, although the experimental points are not given, the broken-line curves indicate where the points are. The pressures are actually measured at stations 1 inch apart. Figure 20 shows sample pressures as measured by mercury manometers.

The six runs chosen for pressure plotting have conditions the same or very close to the six cases with condensation-fog pictures shown in figure 26. There are a low and a high stagnation temperature, namely, 590° R and 990° R, for each of two stagnation pressures, 338 and 508 pounds per square inch absolute. There are a low and a high stagnation temperature, 590° R and 977° R, for the stagnation pressure of 1015 pounds per square inch absolute. On each of the three curves is drawn the design isentrope of the nozzle. On this design isentrope are marked off design Mach numbers.

It is to be noted that the static-pressure curves for the high temperatures for each of the three stagnation pressures level off at a Mach number of approximately 6.8 and that the experimental deviations of the points on this curve are not markedly different for the three different pressures. These correspond to runs in which no condensation fog is detected. On the other hand, the static-pressure curves for the low-temperature runs at each of the three different stagnation pressures show a marked change in the location and some change in the magnitude of the

point at which the sudden pressure rise occurs. Percentagewise, the magnitude of the pressure bump for the low-temperature cases is about the same at all three pressures.

Schlieren Photography

Figure 21 shows composite schlieren photographs of most of the nozzle and test section, extending right down to the nozzle throat, taken at a stagnation temperature of 543° R and stagnation pressures of 1015, 508, and 338 pounds per square inch absolute. Of most interest in these three pictures is the disturbance which starts at about $1/4$ inch from the throat, crosses in the center of the channel at from 2 to 3 inches from the throat and strikes the boundary layer and wall, and is reflected at about 8 to 10 inches from the throat. This point of striking the walls at 8 inches for the high pressure of 1015 pounds per square inch absolute and at about 10 inches for the low pressure of 338 pounds per square inch absolute agrees with the static wall pressure plots of figure 27.

The boundary-layer growth in the nozzle and test section can be seen. Also a complicated system of shock waves off the total-head pressure rake near the end of the test section can be seen. The effect of striations in the Pyrex glass are clearly visible.

Wedge Shock-Wave Measurements

Figure 28 shows schlieren photographs of the shock-wave and boundary-layer pattern obtained using a wedge of 11° total angle. The Mach number before the shock is computed using the relation

$$M = \frac{\left[\frac{5 \frac{\tan \alpha}{\tan (\alpha - \omega)}}{6 - \frac{\tan \alpha}{\tan (\alpha - \omega)}} \right]^{1/2}}{\frac{1}{\sin \alpha}}$$

where α is the half angle of the shock and ω is the deflection of the stream in passing through the shock. Using the wedge half angle of 5.50° for ω , the Mach number calculated is low. If, however, ω includes also the boundary layer as measured from these schlieren photographs, higher Mach numbers result, as shown in figure 28.

A series of wedge shock-wave photographs was taken in a series of runs in which the stagnation pressure was kept constant but in which the stagnation temperature was varied. In figure 29 two such series of runs are plotted with shock wave half angle α plotted against stagnation temperature, one series being at a stagnation pressure of 34.6 atmospheres and the other, at a pressure of 68.6 atmospheres. These series show that the shock angle, hence the Mach number, remains constant at high values of the stagnation temperatures but that a break in the curve comes as the stagnation temperature is lowered and the shock angle becomes larger or the Mach number becomes smaller. This break in the curve is interpreted as the onset of condensation in the air stream.

In all cases the wedge is located at pressure tap 15 in the test section, a position at which the supporting arm is reasonably short, hence free from vibration.

DISCUSSION

Many of the theoretical and experimental results of this investigation are summarized in figure 30 and figure 31. In figure 30, the condensation rate lines of 0, 1, and 10^6 per second are plotted for nitrogen, as calculated from the theory modified to take into account the variation of surface tension with surface curvature. These rate lines are the same as those plotted in figure 12.

Five experimental points are plotted in figure 30. The solid and open circles represent cases in which condensation was detected by light scattering. The points are plotted on isentropes corresponding to the partial pressure of nitrogen in the air. The Mach number as listed in the table in the figure was calculated for the circles from the area ratio corrected by wall static-pressure measurements as described in the previous section. In each of these cases dry air was used. The stagnation conditions for the open circle were 68.6 atmospheres pressure and 293° K temperature; for the solid circle, 34.6 atmospheres pressure and 417° K temperature. The Mach numbers were: For the open circle, 4.45; for the solid circle, 6.32. It is to be noted that these two points fall on rate lines in the range from 10^2 to 10^6 . The rates are changing so rapidly with Mach number that an exact determination is probably not important. Although the isentropic lines are not shown on the graph, the adiabatic supercooling for these two points is 9° or 10° C.

Also in figure 30 are plotted two triangles representing the points at which condensation was detected by the change in the shock angle from

an 11.0° wedge as the stagnation temperature was changed. These measurements were described in the preceding section. The two points are obtained from the data plotted in figure 29. The stagnation conditions for the open triangle are 68.6 atmospheres pressure and 485° K temperature and for the solid triangle, 34.6 atmospheres and 384° K. Mach numbers at which the change in shock angle was detected are 6.7 and 6.5, respectively. It is noted that these two points have greater scatter in condensation rates than do the points obtained by condensation-fog measurements, probably because of inaccuracies in measurement of shock-wave and boundary-layer angles.

The square shows the point at which condensation-fog light scattering was detected when carbon dioxide in the dry air was increased from its normal 3 parts in 10,000 to about $8\frac{1}{2}$ parts in 100. Using stagnation conditions of 34.6 atmospheres and 413° K, condensation was detected at a Mach number of 5.76 as calculated by area ratio corrected by wall static-pressure measurements. This is seen to fall very close to the saturation line of nitrogen.

In figure 31 fractional condensation rate lines of 0, 1, and 10^6 per second are plotted for oxygen. Here the same experimental points described above are plotted on the assumption that oxygen is the component that condenses. It is interesting to note that the solid and open circles fall on about the same rate line, about 10^4 per second. These rates are very close to the rates for nitrogen corresponding to the same experimental points. The adiabatic supercooling for oxygen for these points is 14° or 15° K.

A glance at figures 1 and 2 shows that the condensation rates predicted by the unmodified theory at the points where condensation is experimentally detected are very low, of the order of 10^{-3} per second or less for nitrogen.

The experimental and theoretical results presented in figure 30 and figure 31 bear on an important question in the condensation of air in hypersonic wind tunnels. Because the unmodified theory predicted negligible rates at points where condensation was evidently present in experimental determination by light scattering, static-pressure measurements, and changes in wedge shock-wave angle, the general interpretation has been made by many workers in the field that the condensation detected was not the condensation of oxygen and nitrogen on spontaneously formed nuclei of oxygen and nitrogen but was oxygen and nitrogen condensation on nuclei of impurities such as water vapor and/or carbon dioxide. The evidence presented here does not eliminate this possibility but it does bring back the possibility that the experimentally detected condensation is onto nuclei of nitrogen and oxygen

instead of on impurities. This, of course, is based on the acceptability of the modified theory presented here, which takes into account a change in surface tension with decreasing radius of drop. It is generally agreed that some modification of the theory is needed since the drops which act as nuclei are always so small.

Another question of interest in the condensation of air in hypersonic wind tunnels is the effect of condensation on the static pressures. In figure 27 measured static wall pressures are compared for runs at high stagnation temperatures (approx. 550° K), where there is no condensation, with runs at low stagnation temperatures (approx. 330° K) where condensation is present. In addition, the calculated static wall pressures for the nozzle are plotted. It is seen that the runs without condensation do not deviate radically from the calculated isentrope, although it is apparent that the effective area ratio of the expansion is slightly smaller than that calculated, and the static pressures begin to deviate somewhat at a calculated Mach number between 5.5 and 6.0 or lower.

On the other hand, runs with condensation present deviate much more radically from the calculated isentrope, and, moreover, the deviation increases proportionately with pressure. This is tentatively interpreted to be due to the increasing amount of condensation with increasing pressure as illustrated in figures 25 and 26.

Of interest is the marked jump in static wall pressure which occurs at a station somewhere between the stations 8 and 11 inches from the throat. It is noted that the disturbance remains in the same place with an increase in stagnation pressure from 338 to 1015 pounds per square inch absolute for the hot runs in which condensation does not occur. However, in the cold runs in which condensation does occur and increases with stagnation pressure, the static-wall-pressure disturbance also increases proportionately with stagnation pressure. Furthermore, the disturbances move upstream beginning at the $10\frac{1}{2}$ -inch station for the pressure of 338 pounds per square inch absolute, changing to about the 9-inch station for 508 pounds per square inch absolute and to the $8\frac{1}{2}$ -inch station for 1015 pounds per square inch absolute.

Reference to the schlieren photographs in figure 21 shows that this jump in wall static pressure is caused by a disturbance which has its origin very close to the throat. For the lower-temperature runs in figure 27 the condensation begins very close to the throat, within about $1/4$ inch. A much smaller disturbance originating near the throat is detected in schlieren photographs of higher-temperature runs where condensation is absent. The smaller increase in wall static pressure caused by these smaller disturbances can be detected where they strike

the wall at approximately 11 inches from the throat in the high-temperature runs plotted in figure 27.

It is not possible from these data to determine whether the larger jump in wall static pressure in the low-temperature runs is due to condensation, for there may be another temperature-sensitive phenomenon occurring near the throat, such as boundary-layer separation and reattachment.

Another point of interest, and a matter for argument among workers in the field, relates to the time lags in the initiation of condensation. Under the conditions used in the experiments reported herein, time lags of condensation initiation seem entirely negligible once the supersaturated state conducive to condensation has been reached, as is shown in figure 23, where condensation was detected within $1/4$ inch from the throat.

CONCLUDING REMARKS

The experimental work on condensation-fog light scattering, pressure measurements, and change in wedge shock angles in a hypersonic wind tunnel with a Mach number of approximately 7 has shown condensation of the principal components of air to be present at modest degrees of supersaturation of air. Preheating the air so that it never reaches a supersaturated state or reaches only a slightly supersaturated state prevents the condensation from taking place.

Modification has been made of the usually employed condensation nucleation theory to take account of a postulated decrease of surface tension with decreasing size of nucleus. The resulting predictions of condensation rates fit well the observed experimental results on the assumption that the condensation is initiated by the formation of nuclei of oxygen or nitrogen. Neither the theory nor the experimental work has precluded the possibility that the observed condensation takes place on nuclei of water vapor, carbon dioxide, or other impurities, and further experimental work will be needed. However, the modification of the theory, with its new prediction of higher condensation rates, indicates that such condensation onto nuclei of impurities is not necessarily the explanation of the relatively low supersaturation ratios reached before condensation starts.

Time lags in the initiation of condensation were found to be negligible once the air had reached a supersaturated state sufficient to start condensation according to the modified nucleation theory.

The effect of the condensation of air on static wall pressures was marked. Some evidence, though by no means conclusive, was presented to show that a condensation shock is present.

Massachusetts Institute of Technology
Cambridge, Mass., November 3, 1950

APPENDIX A

DERIVATION OF APPROXIMATE EXPRESSION FOR VARIATION OF SURFACE
ENERGY PER UNIT SURFACE WITH SURFACE CURVATURE

It is assumed that the expression for the surface energy per unit surface depends on the radius of curvature of the surface as

$$w = \sigma_{\omega} f(r)$$

Here $f(r)$ will be derived on the basis that the number of closest neighbors of a surface molecule determines the surface energy per unit surface. A simple geometrical picture will be used.

Referring to figure 32 it is assumed that there is a drop of liquid containing many similar spherical molecules. (Three are shown in fig. 32). Let r_c be the radius from the center of the drop to the center of the surface molecules and r , the radius from the center of the drop to the periphery of the molecules. The half cone angle of the solid angle ω containing all the nearest neighbors to the surface molecule is α . The solid angle ω containing nearest neighbors is given by

$$\omega = 2\pi(1 - \cos \alpha)$$

It is seen from the construction that

$$\alpha = \frac{2}{3}\pi - \frac{\theta}{2}$$

Hence

$$\omega = 2\pi \left[1 - \cos \left(\frac{2\pi}{3} - \frac{\theta}{2} \right) \right]$$

$$\omega = 2\pi \left(1 - \cos \frac{2\pi}{3} \cos \frac{\theta}{2} - \sin \frac{2\pi}{3} \sin \frac{\theta}{2} \right)$$

Further, from the construction

$$\sin \frac{\theta}{2} = \frac{D}{2r - D}$$

$$\cos \frac{\theta}{2} = \frac{2\sqrt{r^2 - rD}}{2r - D}$$

Hence

$$\omega = 2\pi \left(1 + \frac{\sqrt{r^2 - rD}}{2r - D} - \frac{\sqrt{3}}{2} \frac{D}{2r - D} \right)$$

From this picture $f(r)$ can be obtained by dividing this solid angle by the solid angle of nearest neighbors when the drop has an infinite radius or $\theta/2 = 0$.

$$\omega \left(\frac{\theta}{2} = 0 \right) = \frac{3}{2}(2\pi)$$

Therefore

$$f(r) = \frac{2}{3} \left(1 + \frac{\sqrt{r^2 - rD}}{2r - D} - \frac{\sqrt{3}}{2} \frac{D}{2r - D} \right) \quad (7)$$

where r is the radius of the drop and D is the diameter of the spherical molecules making up the drop.

REFERENCES

1. Charyk, Joseph V., and Lees, Lester: Condensation of the Components of Air in Supersonic Wind Tunnels. Rep. No. 127, Aero. Eng. Lab., Princeton Univ., March 1, 1948.
2. Bogdonoff, Seymour M., and Lees, Lester: Study of the Condensation of the Components of Air in Supersonic Wind Tunnels. Part I - Absence of Condensation and Tentative Explanation. Rep. No. 146, Contract AF 33 (038) - 250, Air Materiel Command, U. S. Air Force, and Aero. Eng. Lab., Princeton Univ., May 25, 1949.
3. Wegener, P.: On the Experimental Investigation of Hypersonic Flow. Memo. No. 9629, Naval Ordnance Lab., July 29, 1948.
4. Wegener, P.: Investigation of Possible Air Condensation in Supersonic Wind Tunnels at High Mach Numbers. Memo. No. 8659, Naval Ordnance Lab., Aug. 1, 1946.
5. Puckett, Allen E.: Hypersonic Wind Tunnel. Progress Rep. No. 4, Contract W-04-200 Ord-1463, Ordnance, Dept. Army, and GALCIT, July 10, 1946.
6. Puckett, A. E., and Schamberg, R.: Hypersonic Wind Tunnel. Progress Rep. No. 5, Contract W-04-200 Ord-1463, Ordnance, Dept. Army, and GALCIT, Aug, 8, 1946.
7. Nagamatsu, H.: Hypersonic Wind Tunnel. Progress Summary to May 15, 1950, Contract W-04-200 Ord-1463, Ordnance, Dept. Army, and GALCIT.
8. Buhler, R. D.: Recent Results on the Condensation Investigation. Contract W-04-200 Ord-1463, Ordnance, Dept. Army, and GALCIT, July 9, 1950.
9. Becker, John V.: Results of Recent Hypersonic and Unsteady Flow Research at the Langley Aeronautical Laboratory. Jour. Appl. Phys., vol. 21, no. 7, July 1950, pp. 619-628.
10. Head, Richard M.: Investigations of Spontaneous Condensation Phenomena. Ph. D. Thesis, C.I.T., 1949.
11. Lukasiewicz, J.: Humidity Effects in Supersonic Flow of Air. Rep. No. Aero. 2211/SD20, British R.A.E., July 1947.
12. Thomson, Sir William, Lord Kelvin: On the Equilibrium of Vapour at a Curved Surface of Liquid. Proc. Roy. Soc. (Edinburgh), vol. VII, no. 80, 1870, pp. 63-68; also Phil. Mag., ser. 4, vol. 42, 1871, pp. 448-452.

13. Von Helmholtz, R.: Untersuchungen über Dämpfe und Nebel, besonders über solche von Lösungen. *Ann. Phys.*, Bd. 27, Heft 4, 1886, pp. 508-543.
14. Becker, R., and Doring, W.: Kinetische Behandlung der Keimbildung in Übersättigten Dämpfen. *Ann. Phys.*, Folge 5, Bd. 24, 1936, pp. 719-752.
15. Volmer, Max: *Kinetik der Phasenbildung*. Theodor Steinkopff (Dresden), 1939.
16. Volmer, M., and Weber, A.: Keimbildung in Übersättigten Gebilden. *Zeitschr. phys. Chemie, Abschn. A*, Bd. 119, Heft 3 and 4, 1926, pp. 277-301.
17. Kaischew, R., and Stranski, I.: Zur Kinetischen Ableitung der Keimbildungsgeschwindigkeit. *Zeitschr. Phys. Chemie, Abschn. B*, Bd. 26, Heft 4 and 5, 1934, pp. 317-326.
18. Farkas, L.: Keimbildungsgeschwindigkeit in Übersättigten Dämpfen. *Zeitschr. Phys. Chemie, Abschn. A*, Bd. 125, Heft 3 and 4, 1927, pp. 236-242.
19. Zeldovich, Y. B.: Theory of the Formation of a New Phase Cavitation. *Jour. Exp. and Theoretical Phys. (USSR)*, vol. 12, 1942, pp. 525-538.
20. Frenkel, J.: *Kinetic Theory of Liquids*. The Clarendon Press (Oxford), 1946.
21. Cwilong, B. M.: Sublimation in a Wilson Cloud Chamber. *Proc. Roy. Soc. (London)*, ser. A, vol. 190, no. 1020, June 17, 1947, pp. 137-143.
22. Anon.: *Landolt-Börnstein Physikalisch-Chemische Tabellen*. Vol. I. Fifth ed., Walther A. Roth and Karl Scheel, eds., Julius Springer (Berlin), 1923.
23. Aoyama, Shin'ichi, and Kanda, Eizō: The Vapor Tensions of Oxygen and Nitrogen in the Solid State. *Sci. Reps., Tohoku Imp. Univ. Sendai*, vol. 24, 1935, pp. 107-115.
24. National Research Council (Edward W. Washburn, ed.): *International Critical Tables*. Vol. VII. First ed., McGraw-Hill Book Co., Inc., 1930.
25. Hodgman, Charles D., ed.: *Handbook of Chemistry and Physics*. Twenty-eighth ed., Chemical Rubber Pub. Co. (Cleveland), 1944.

26. Hoge, H. J.: Vapor Pressure of Oxygen. NBS-NACA Tables of Thermal Properties of Gases, Table 9.50, Dec. 1949.
27. Kantrowitz, A.: Nucleation in Very Rapid Vapor Expansions. Contributed paper, Div. Fluid Dynamics, Am. Phys. Soc. Meeting, Urbana, Ill., May 12-13, 1950.
28. Tolman, R. C.: Effect of Droplet Size on Surface Tension. Jour. Chem. Phys., vol. 17, no. 3, March 1949, pp. 333-337.
29. Mayer, Joseph Edward, and Mayer, Maria Geoppert: Statistical Mechanics. John Wiley & Sons, Inc., 1940.
30. Kirkwood, J. G., and Buff, F. P.: The Statistical Mechanical Theory of Surface Tension. Jour. Chem. Phys., vol. 17, no. 3, March 1949, pp. 338-343.
31. Stever, H. G.: A Modification of the Theory of Kinetics of Condensation and Its Application to Air Condensation in Hypersonic Tunnels. Contributed Paper, Div. Fluid Dynamics, Am. Phys. Soc. Meeting, Charlottesville, Va., Dec. 28-30, 1949.
32. Busemann, A.: Gasdynamik. Bd. 4, Teil 1 der Handbuch der Experimentalphysik, Ludwig Schiller, ed., Akademische Verlags (Leipzig), 1931, pp. 341-460.
33. Neumann, E. P., and Lustwerk, F.: Supersonic Diffusers for Wind Tunnels. Jour. Appl. Mech., vol. 16, no. 2, June 1949, pp. 195-202.

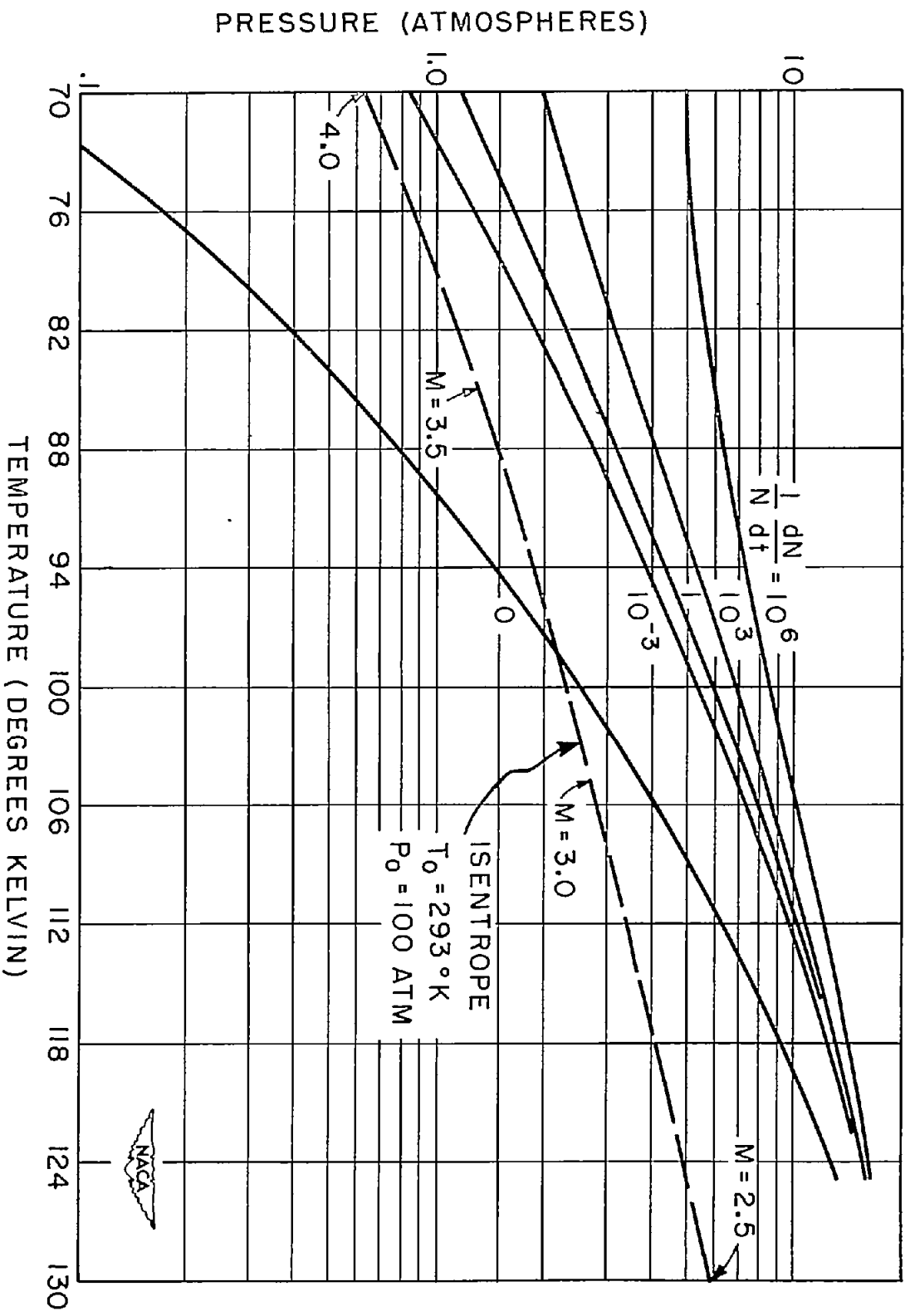


Figure 1.- Oxygen condensation rates - unmodified theory.

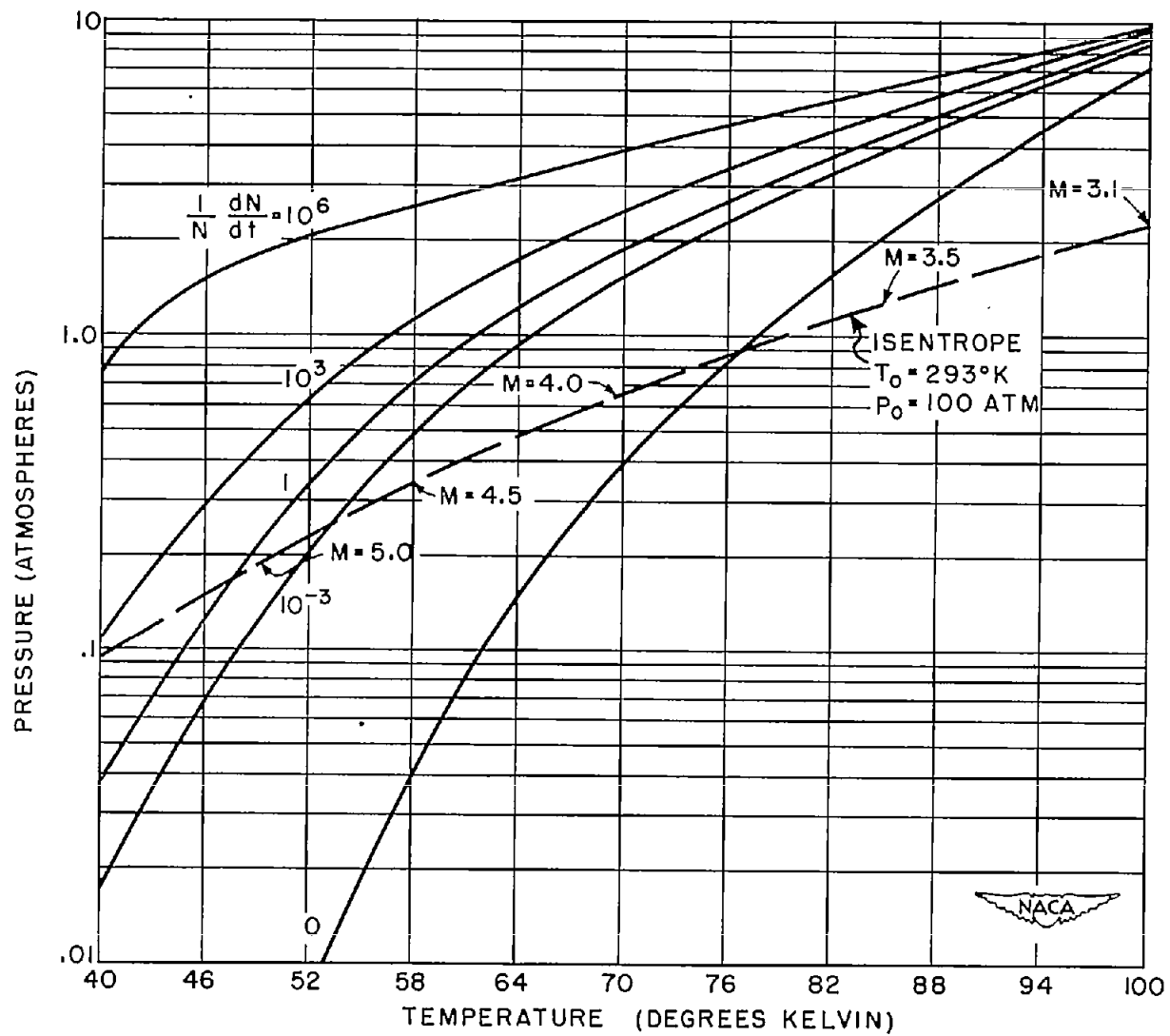


Figure 2.- Nitrogen condensation rates - unmodified theory.

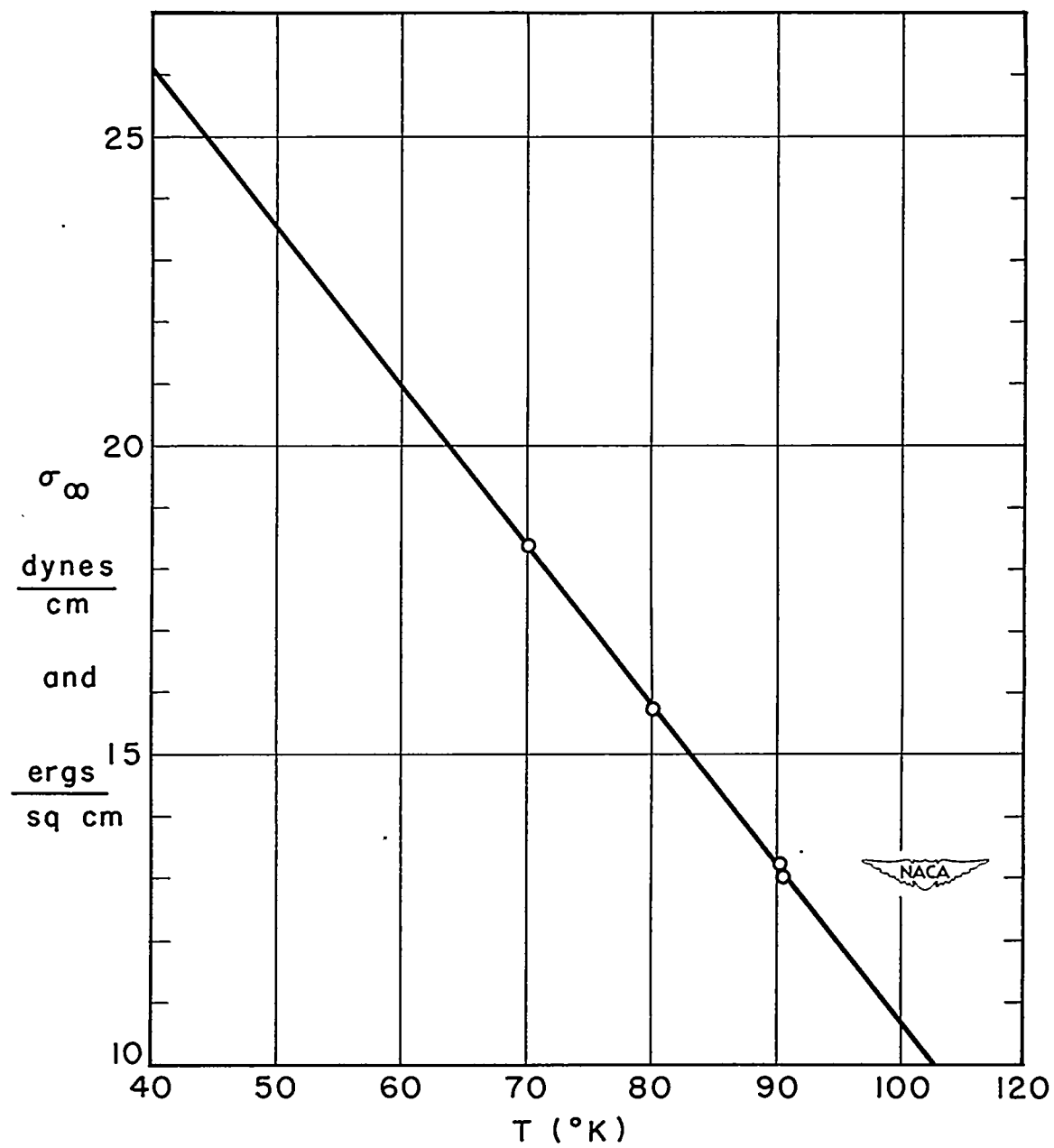


Figure 3.- Surface tension of oxygen against temperature.

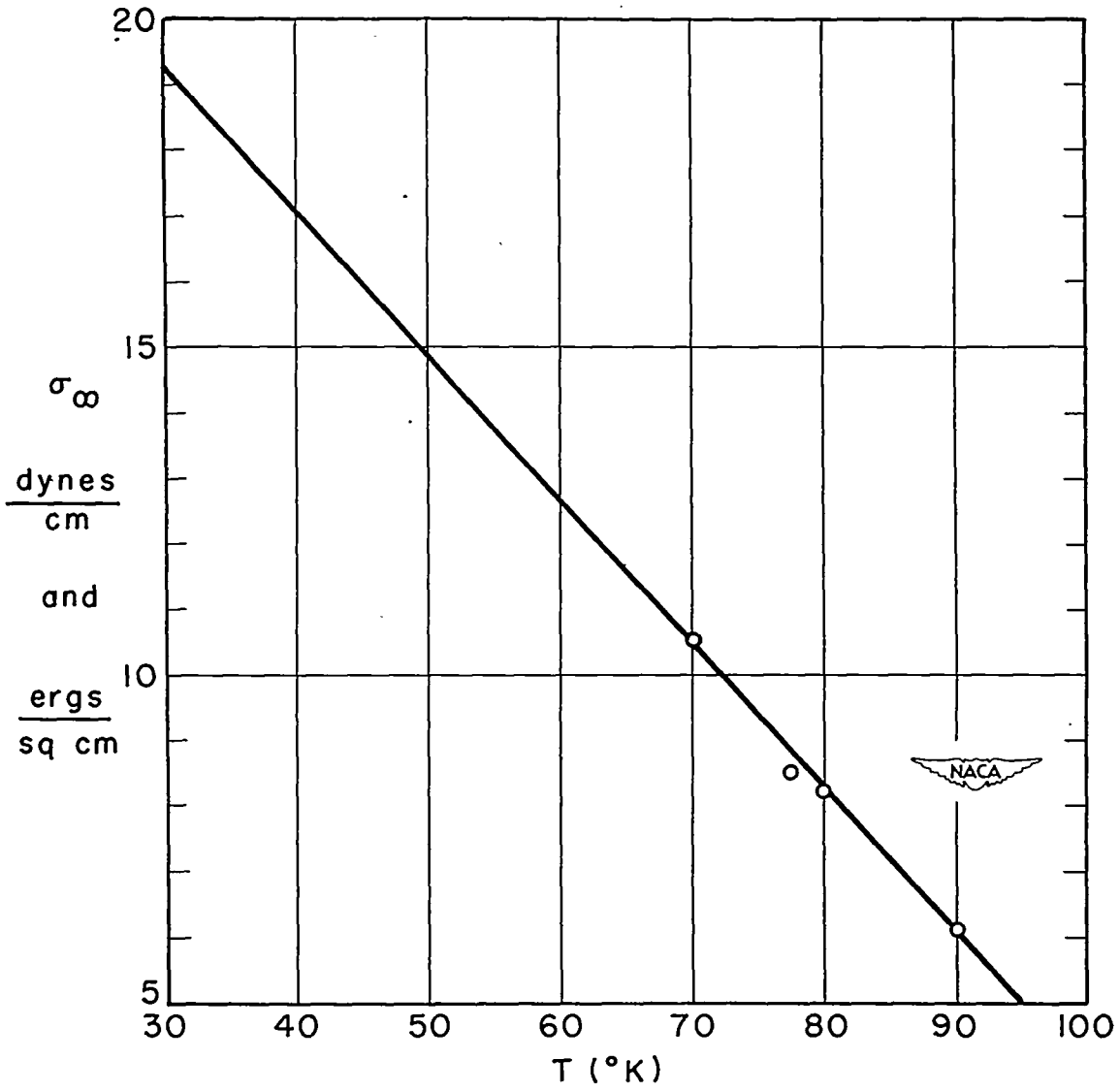


Figure 4.- Surface tension of nitrogen against temperature.

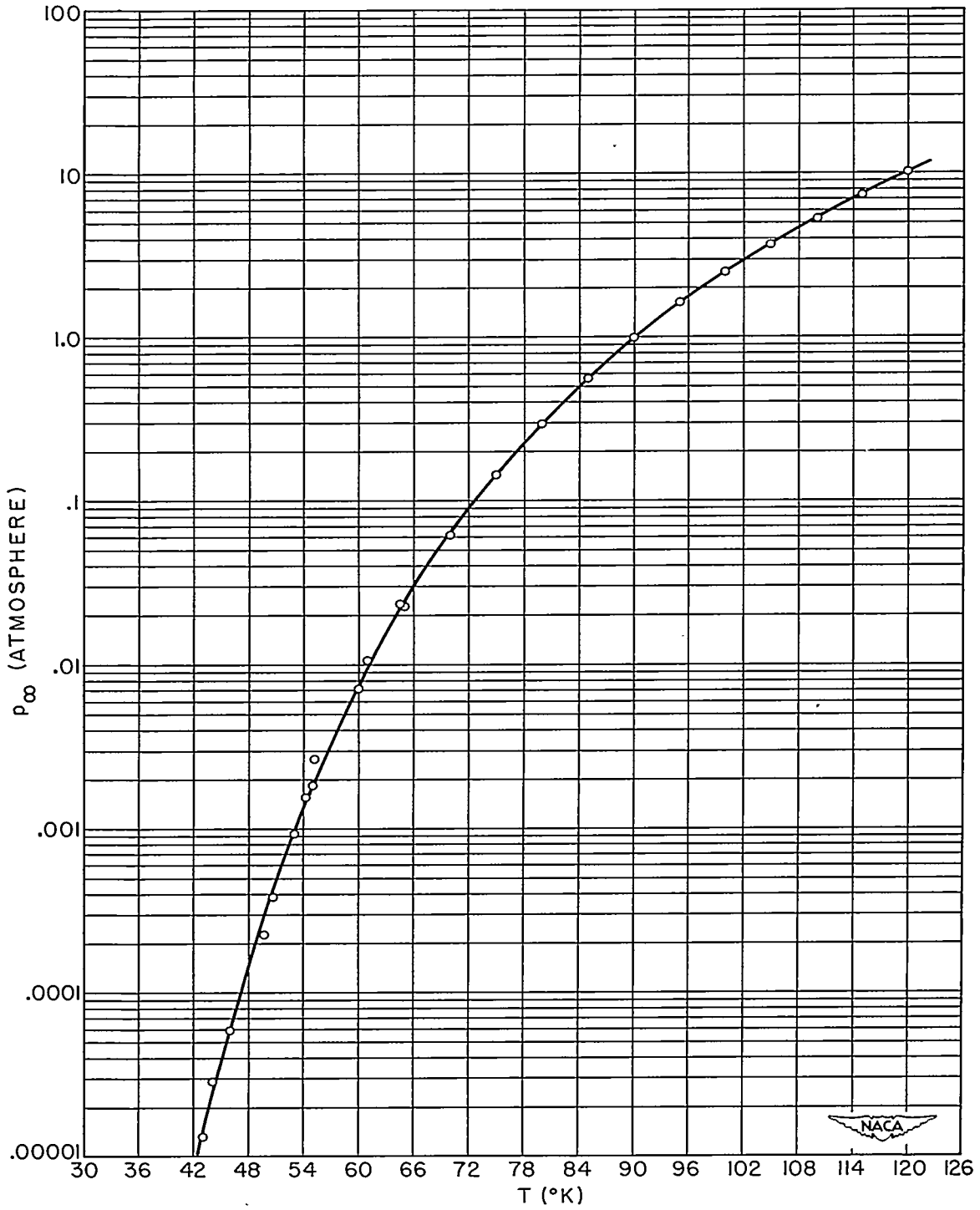


Figure 5.- Vapor pressure of oxygen against temperature.

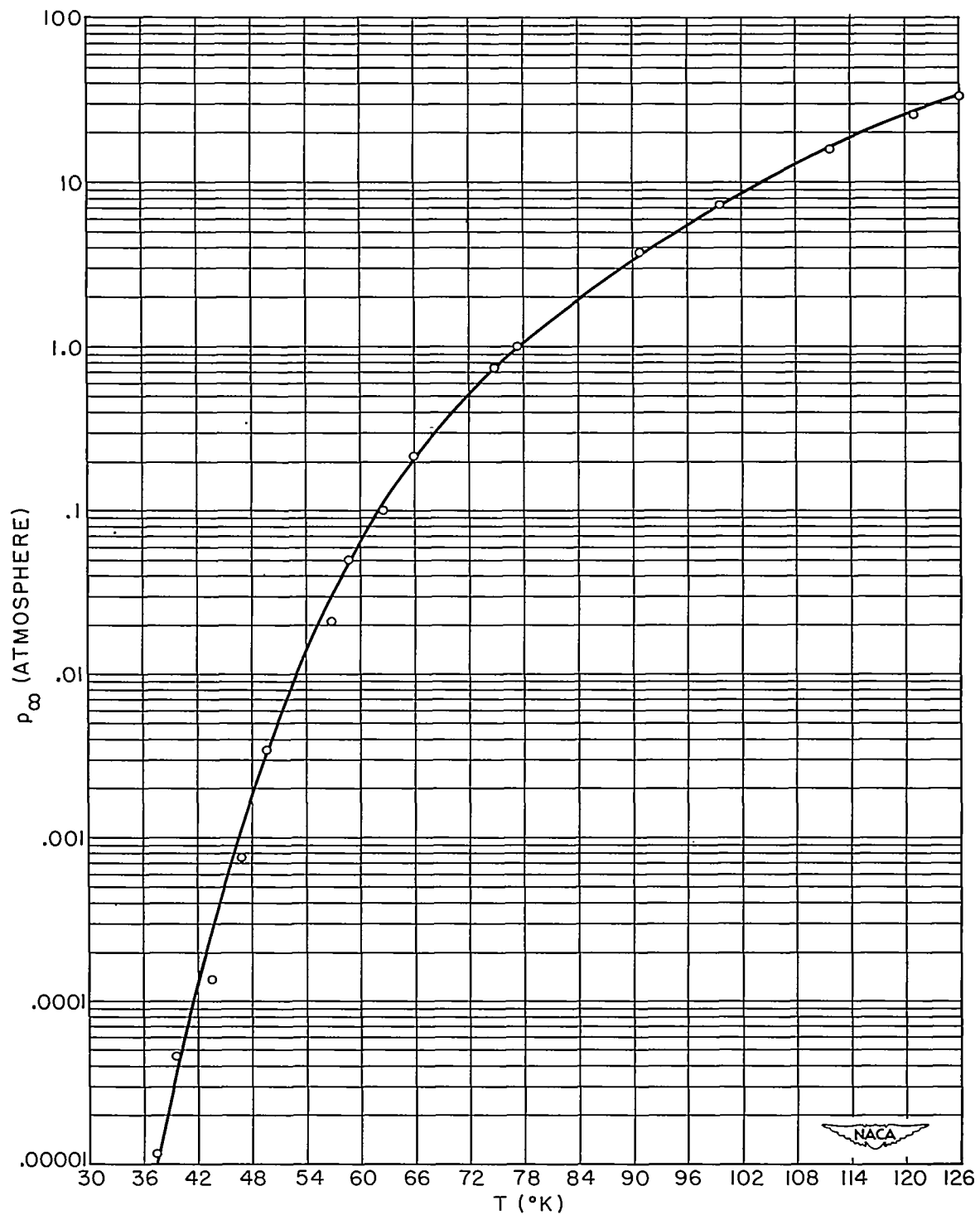


Figure 6.- Vapor pressure of nitrogen against temperature.

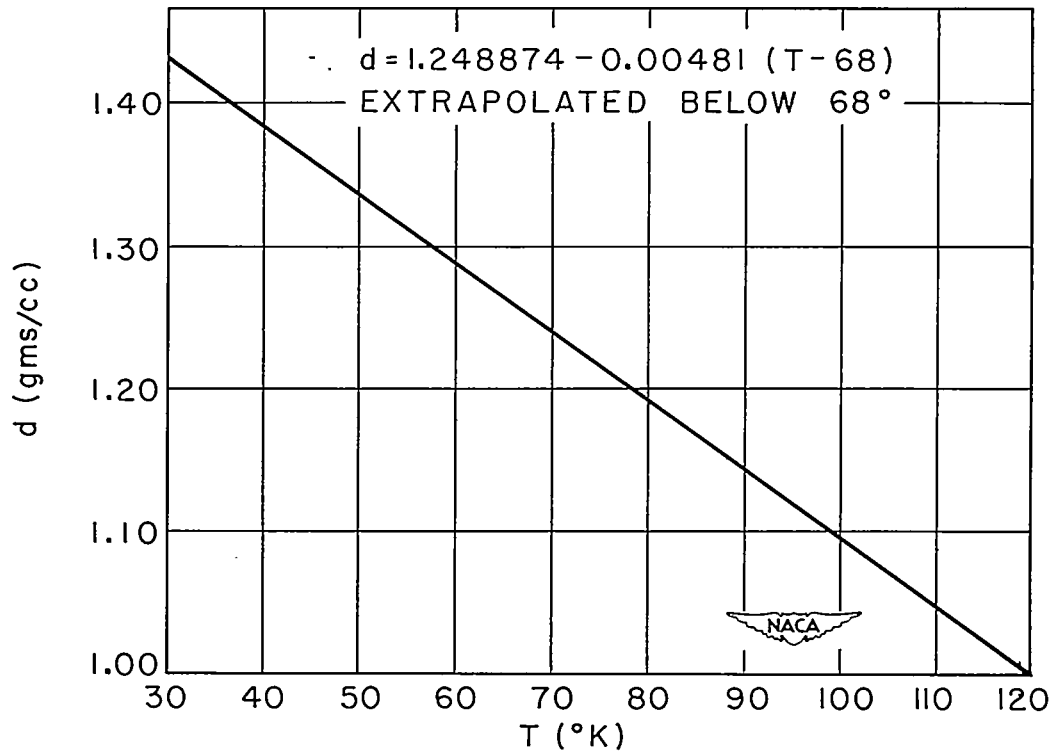


Figure 7.- Density of liquid oxygen against temperature.

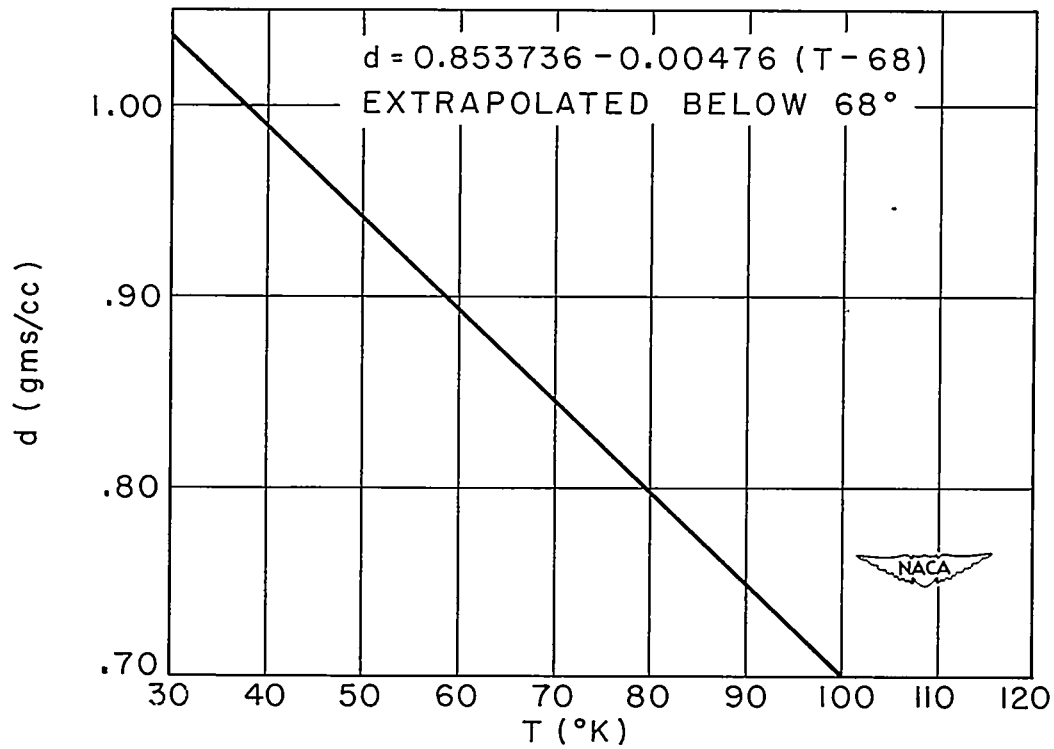


Figure 8.- Density of liquid nitrogen against temperature.

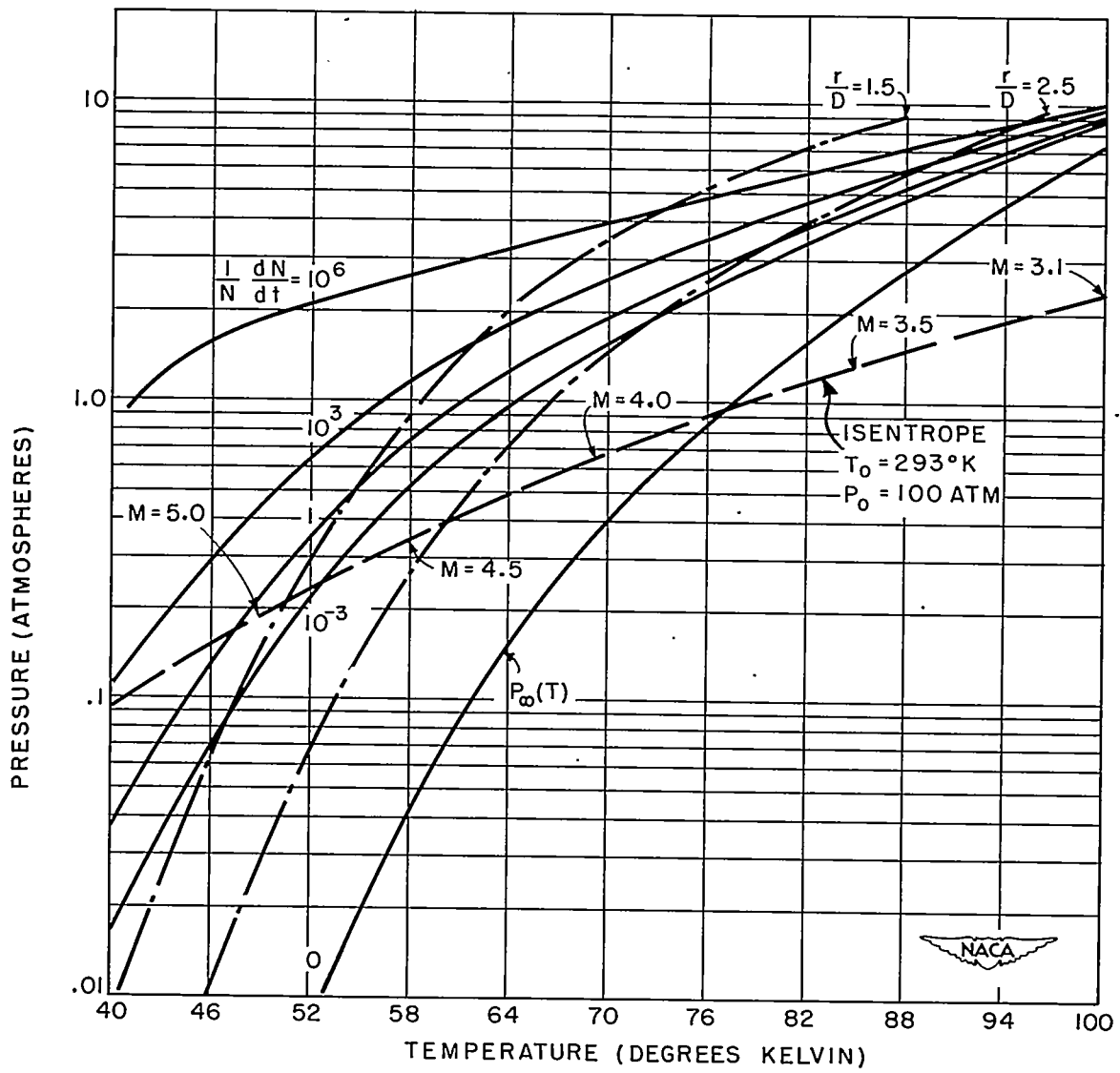
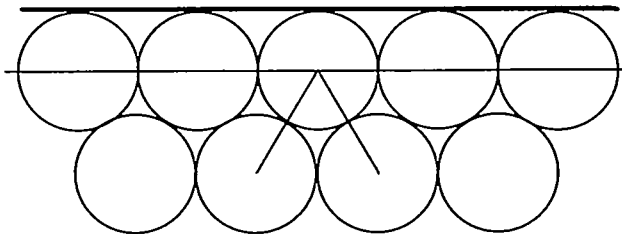


Figure 9.- Nitrogen condensation rates - unmodified theory.

FLAT SURFACE

$$r = \infty$$



DROP SURFACE

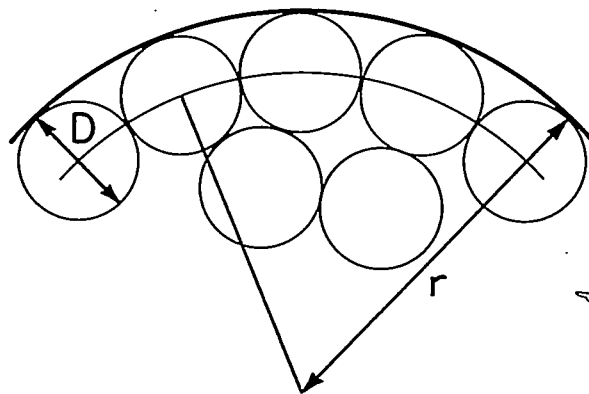
 $r - \text{FINITE}$ 

Figure 10.- Effect of surface curvature on number of closest neighbors for surface molecule.

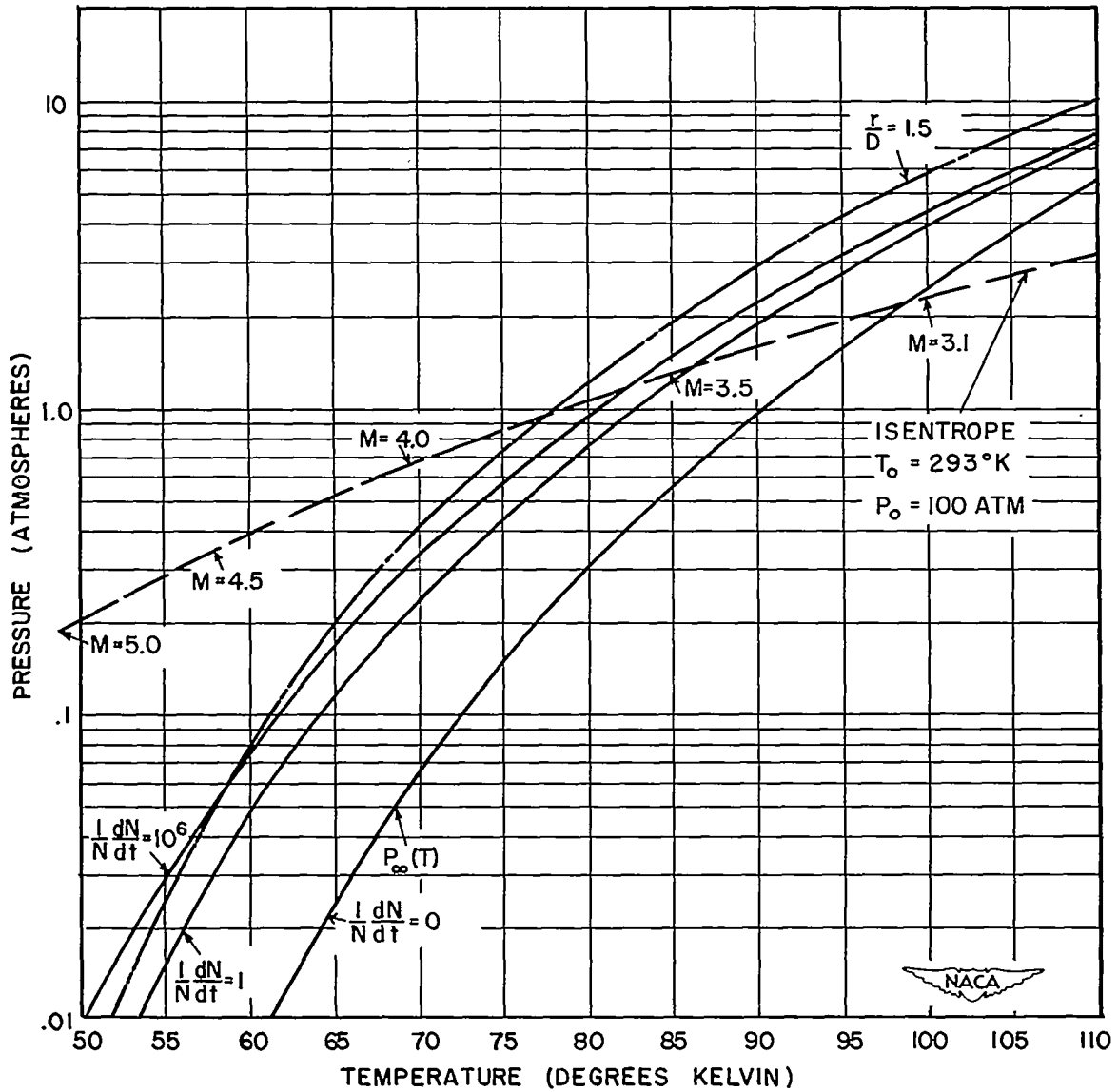


Figure 11.- Oxygen condensation rates - modified theory.

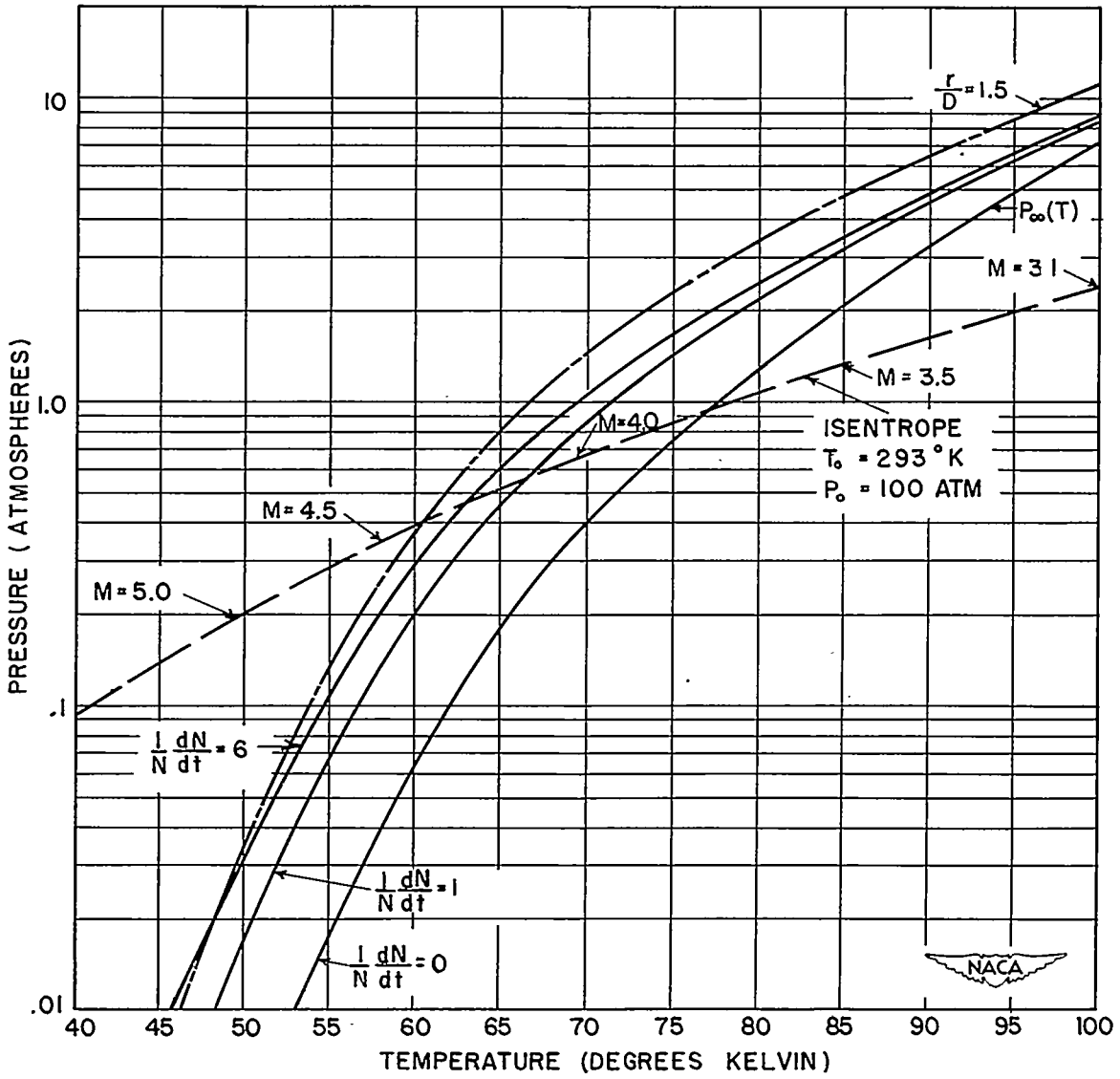


Figure 12.- Nitrogen condensation rates - modified theory.

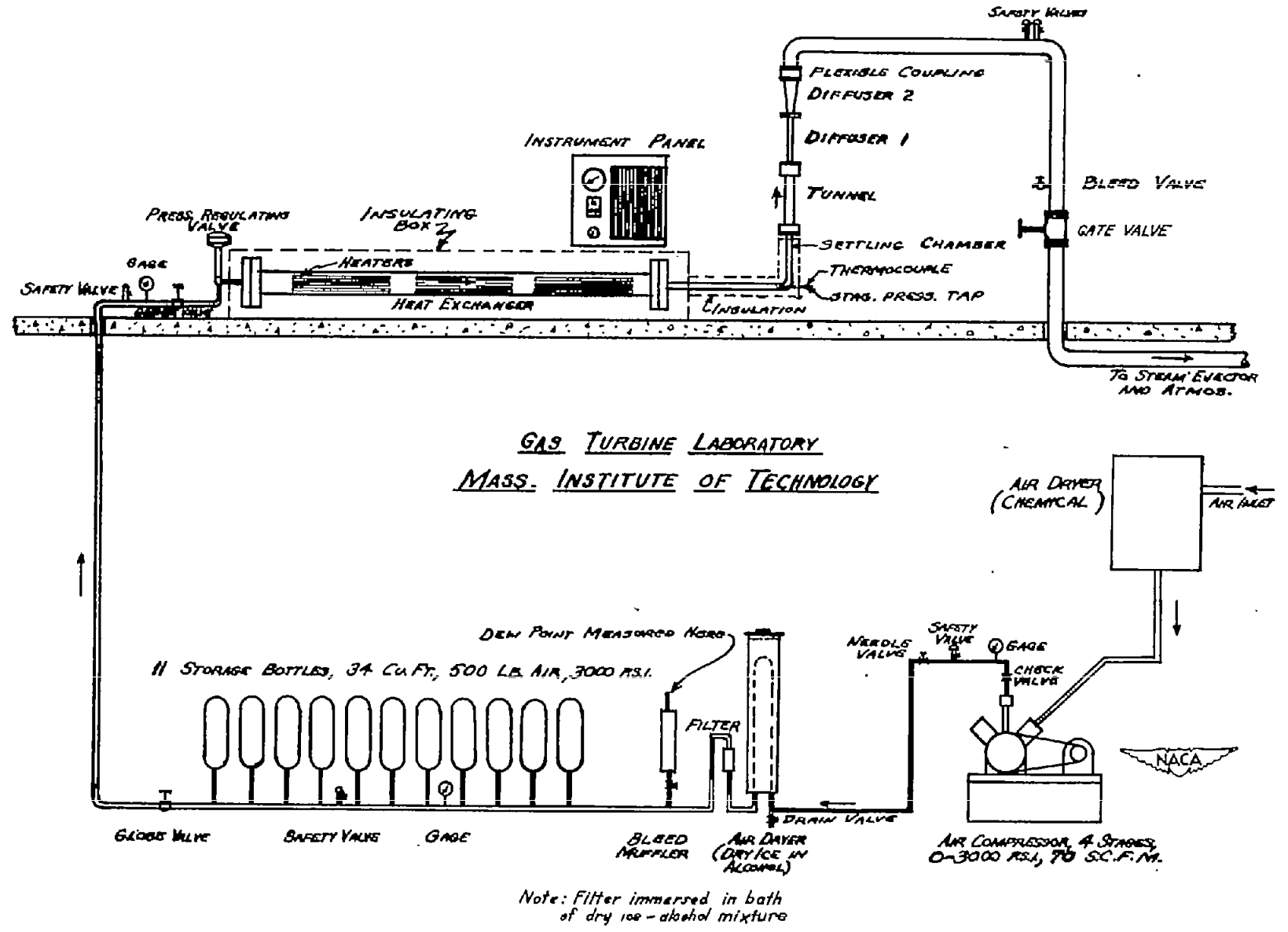


Figure 13.- Schematic diagram of hypersonic wind tunnel.

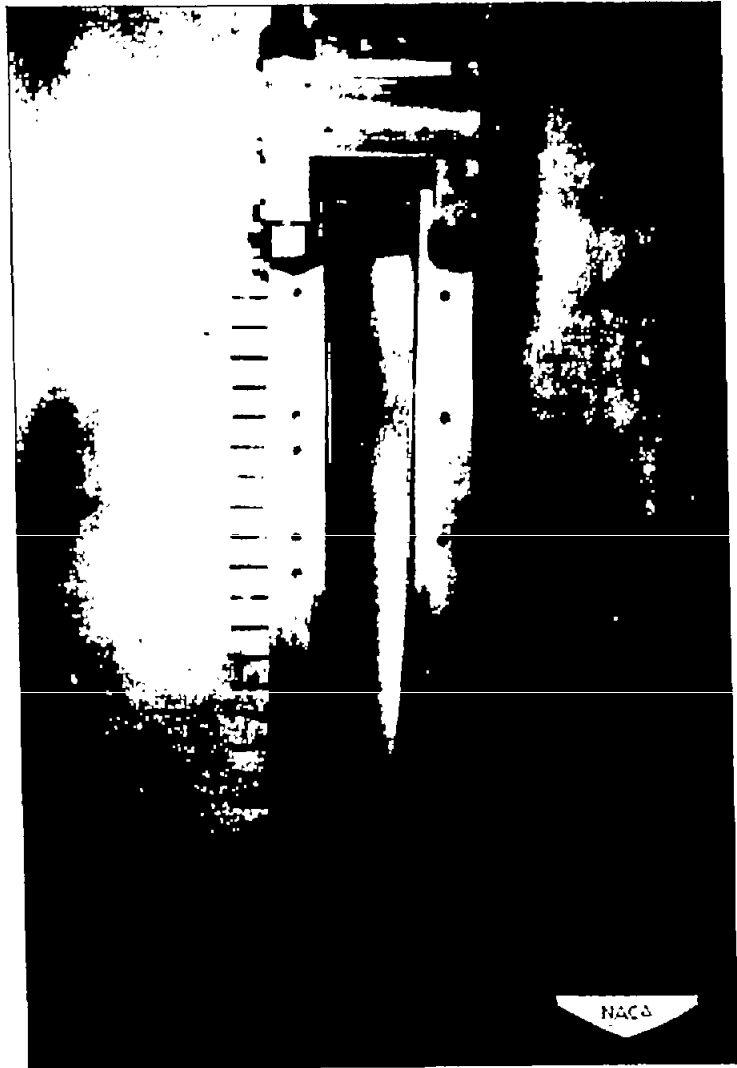
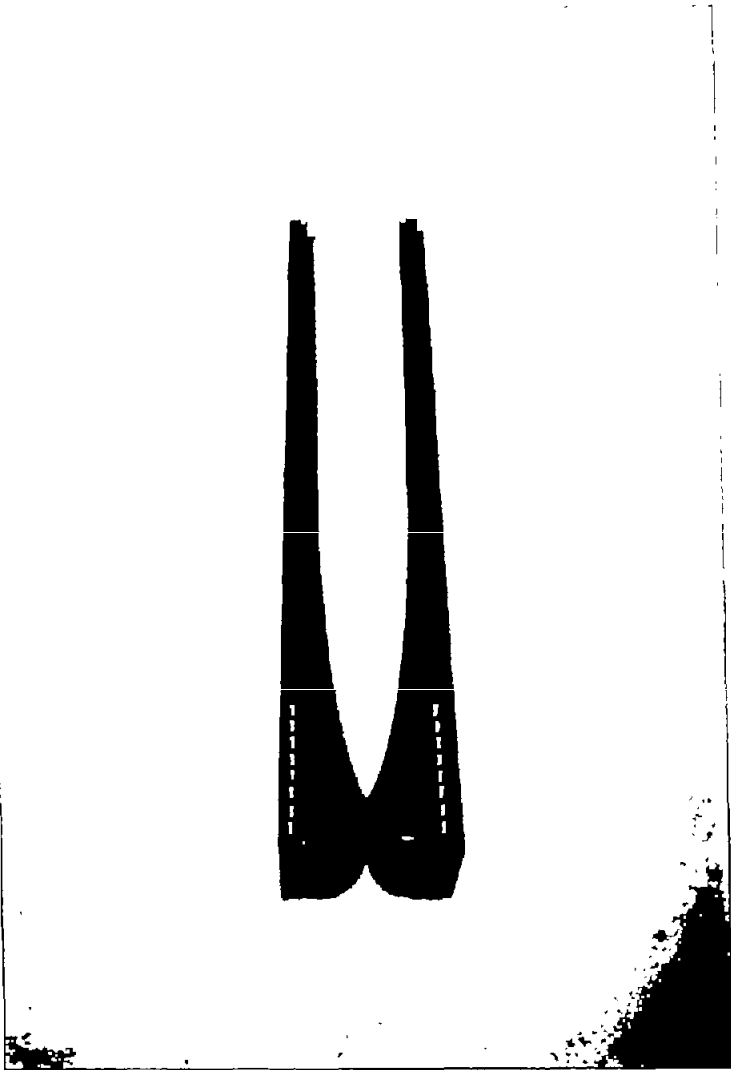


Figure 14.- Nozzle blocks and partial assembly.

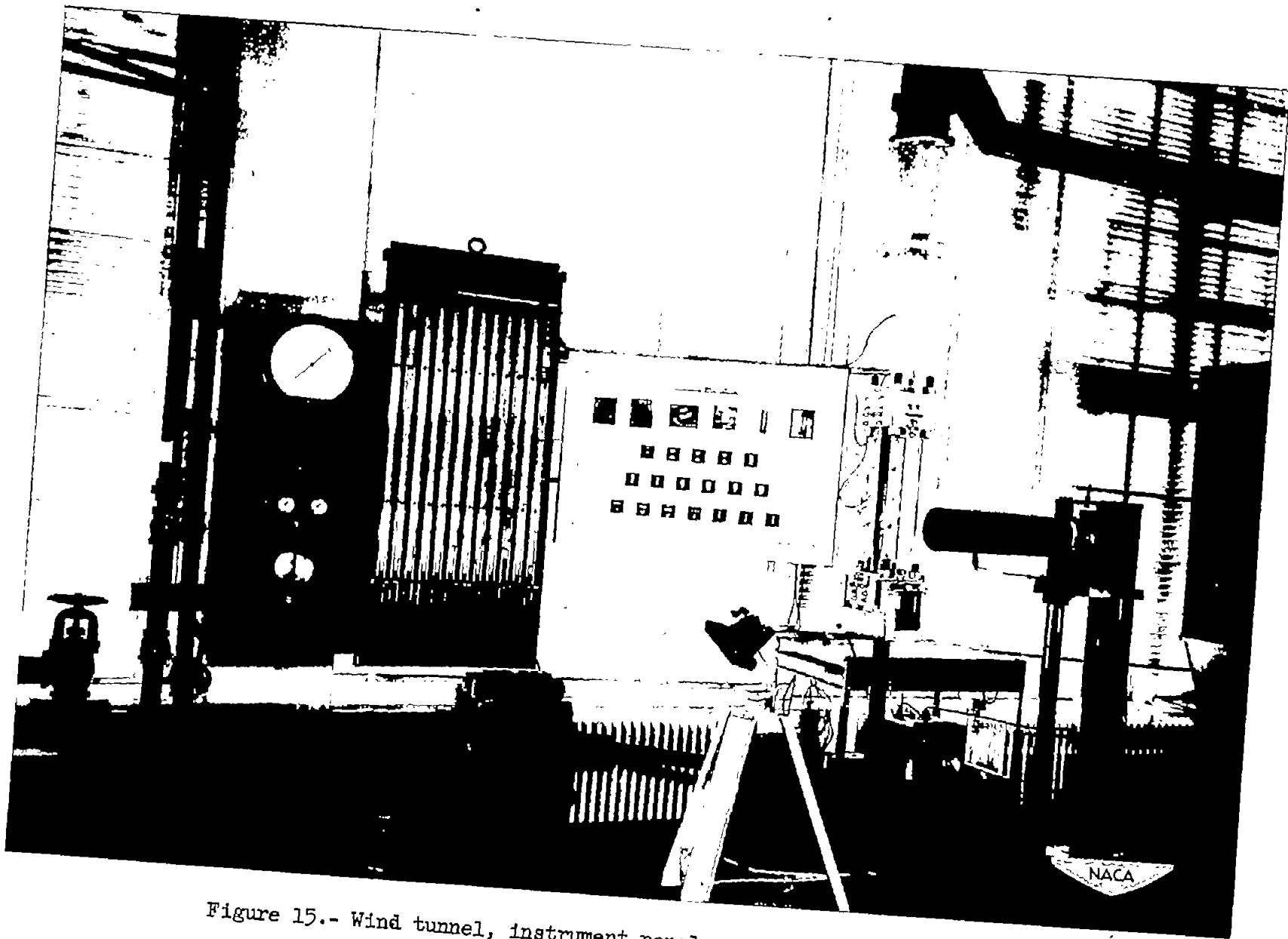
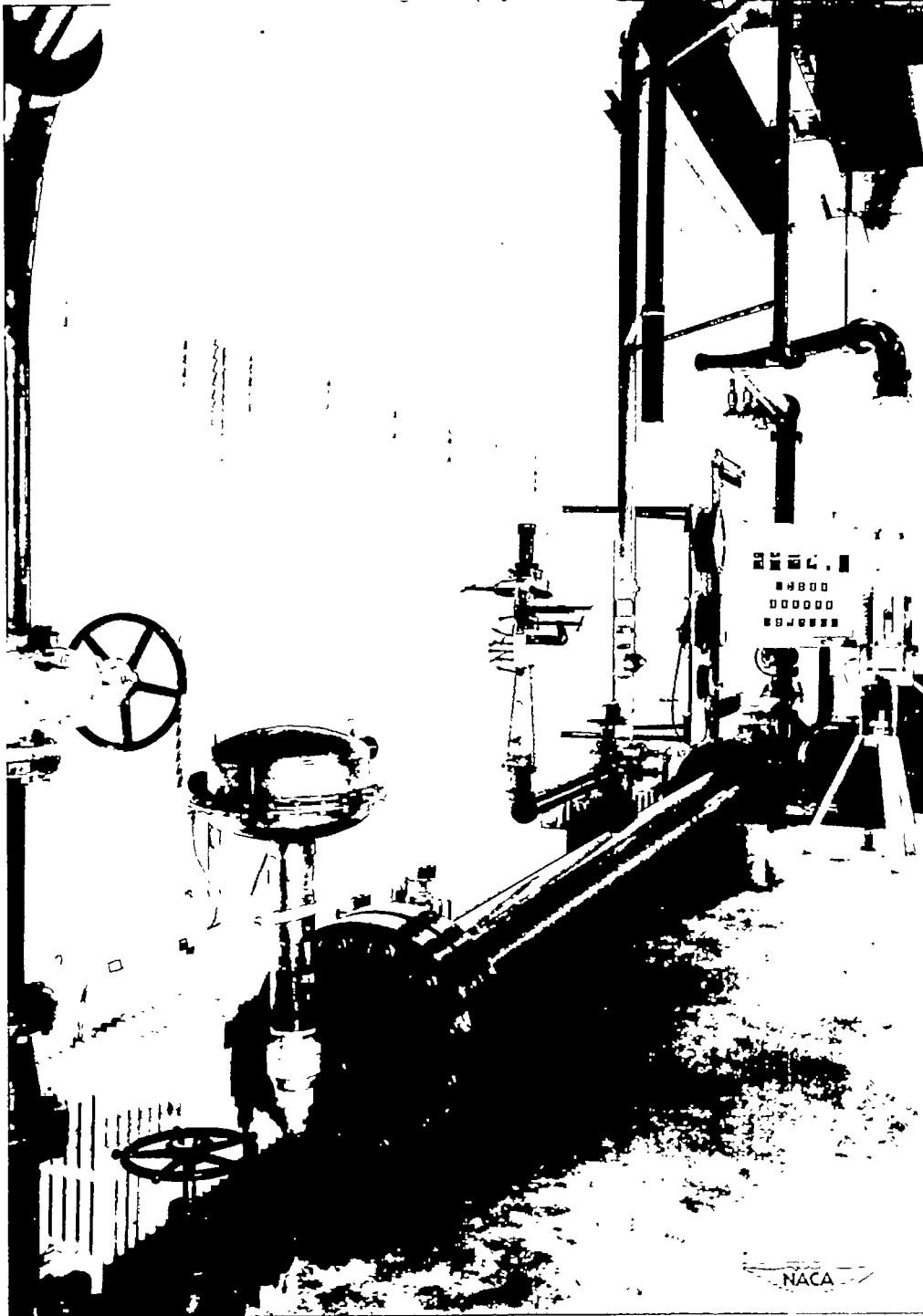
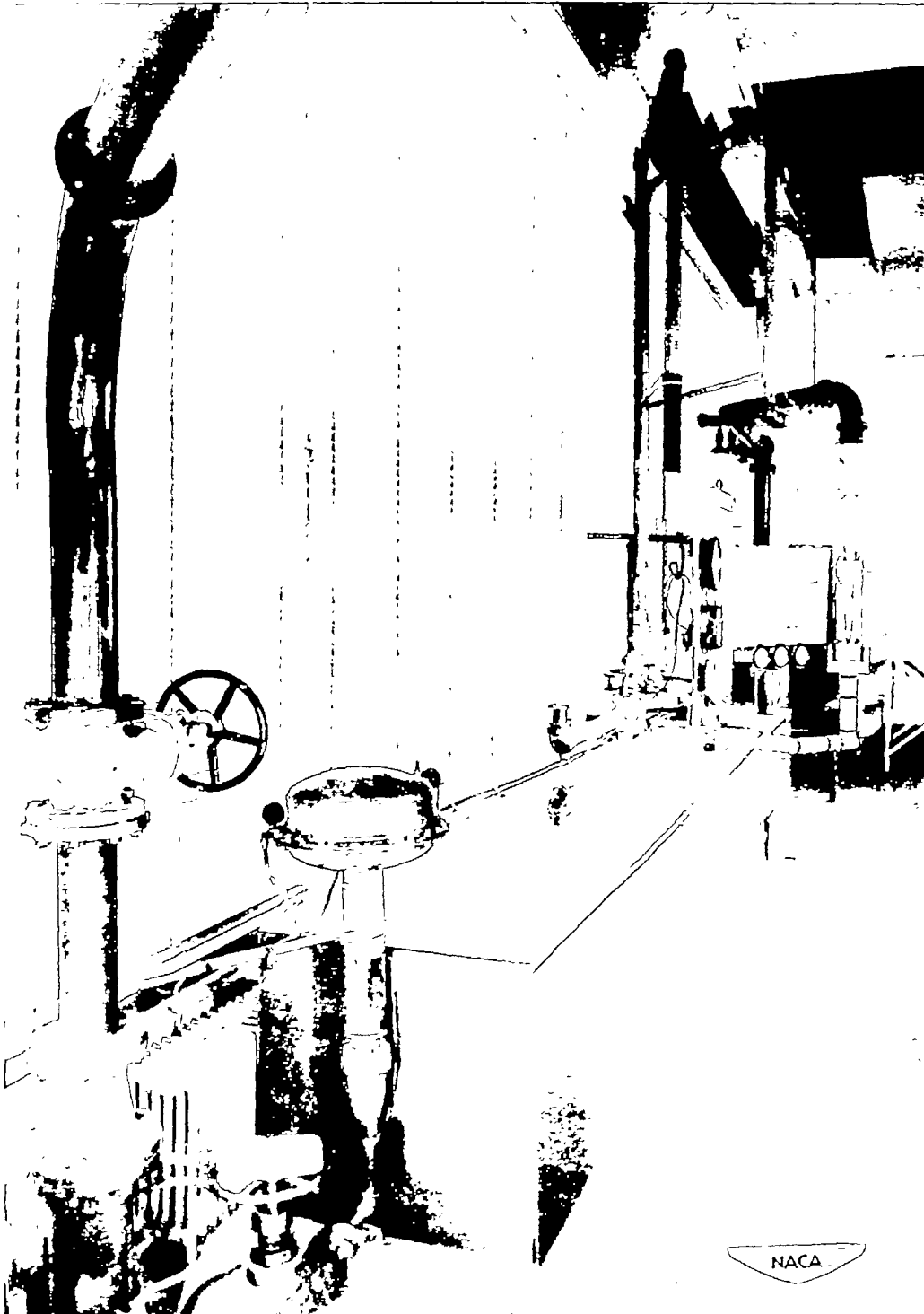


Figure 15.- Wind tunnel, instrument panel, and equipment for making light-scattering photographs.



(a) Before installation of heaters.

Figure 16.- Pressure-regulating valve and heat exchanger.

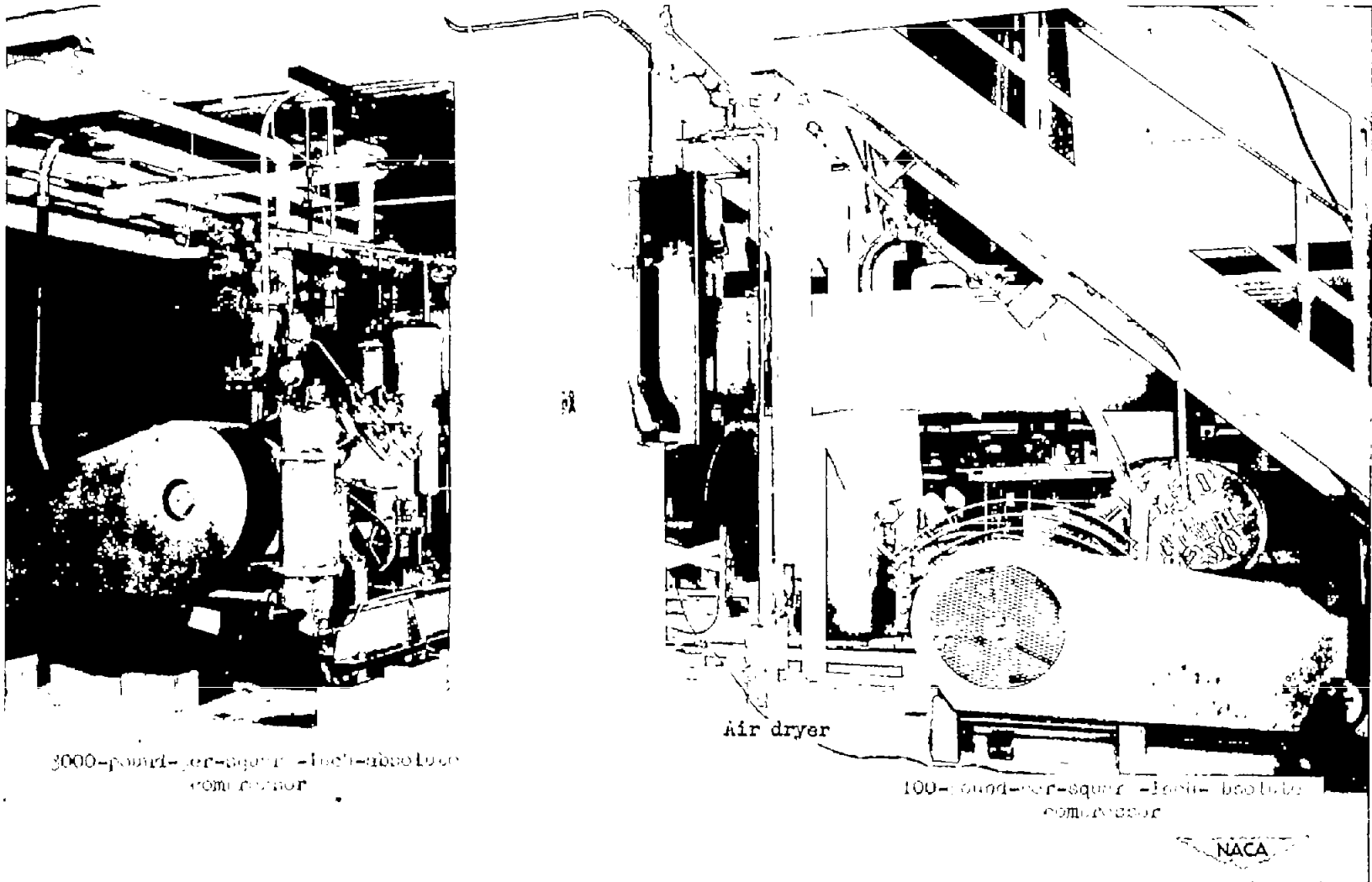


(b) After installation of heaters.

Figure 16.- Concluded.



Figure 17.- Interior of heat exchanger showing $\frac{1}{16}$ -inch aluminum rods.



3000-pound-per-square-foot-absolute
compressor

Air dryer

100-pound-per-square-foot-absolute
compressor

NACA

Figure 18.- Air compressors and air dryer.

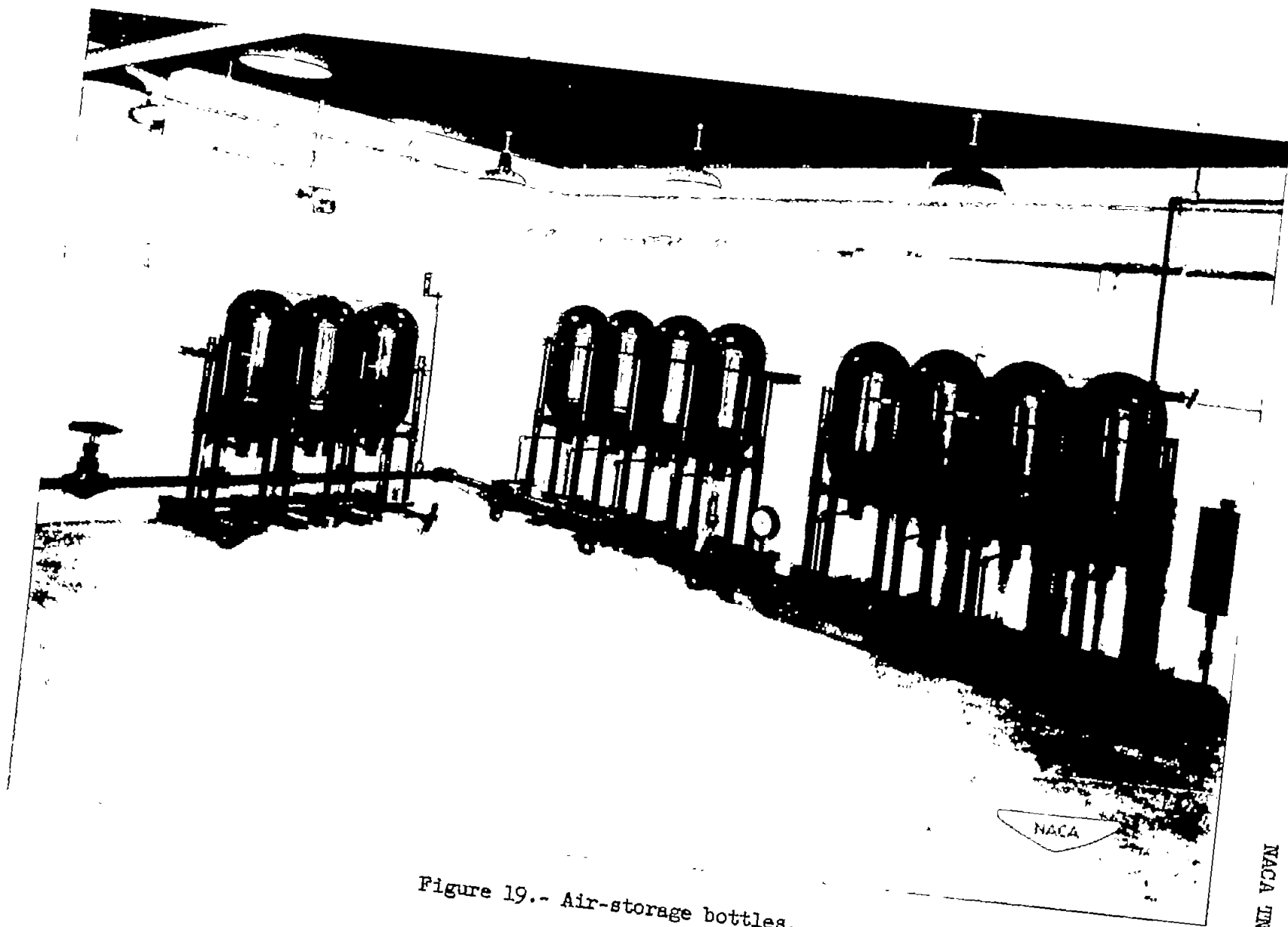
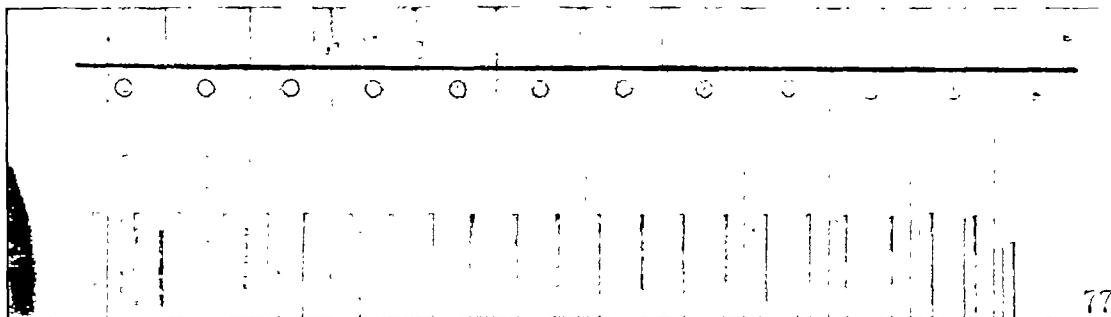


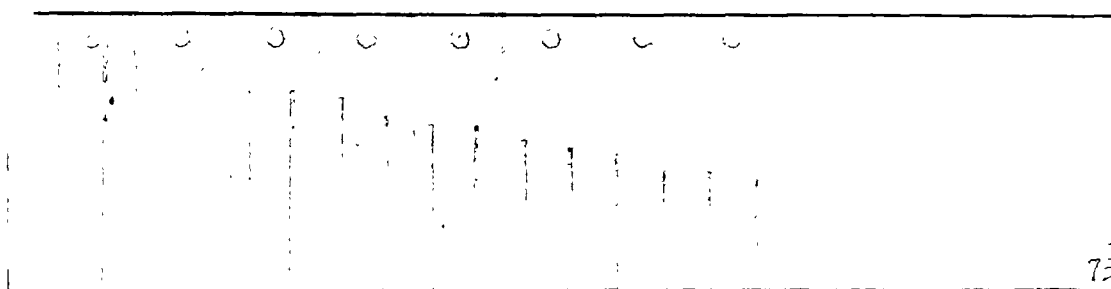
Figure 19.- Air-storage bottles.

NACA TM 2559



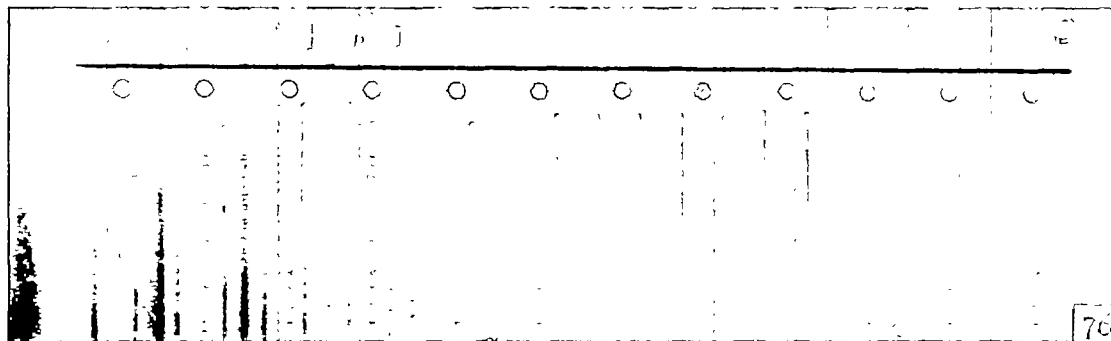
1 2 3 4 5 6 7 8 9 10 11 12 13 14 15 16 17 18 1 2 3 4 5 Ref.
 Probe

(a) No flow.



1 2 3 4 5 6 7 8 9 10 11 12 13 1 15 16 17 18 1 2 3 4 5 Ref.
 Probe

(b) Subsonic after tap 2. $P_o = 300$ pounds per square inch absolute; $T_o = 590^\circ$ R.

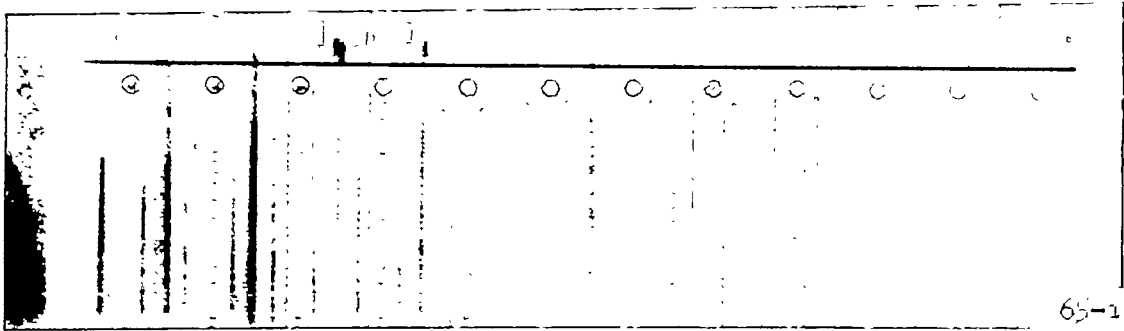


1 2 3 4 5 6 7 8 9 10 11 12 13 14 15 16 17 18 1 2 3 4 5 Ref.
 Probe

(c) $P_o = 1300$ pounds per square inch absolute; $T_o = 590^\circ$ R.

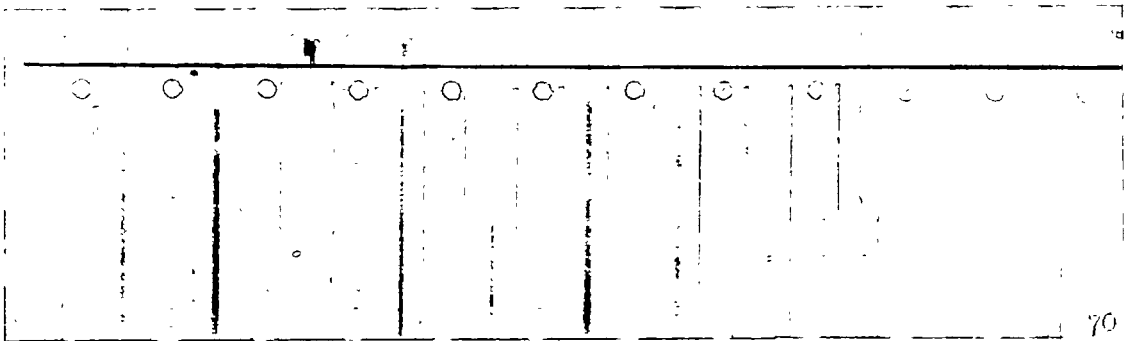


Figure 20.- Manometers at various pressures and temperatures.



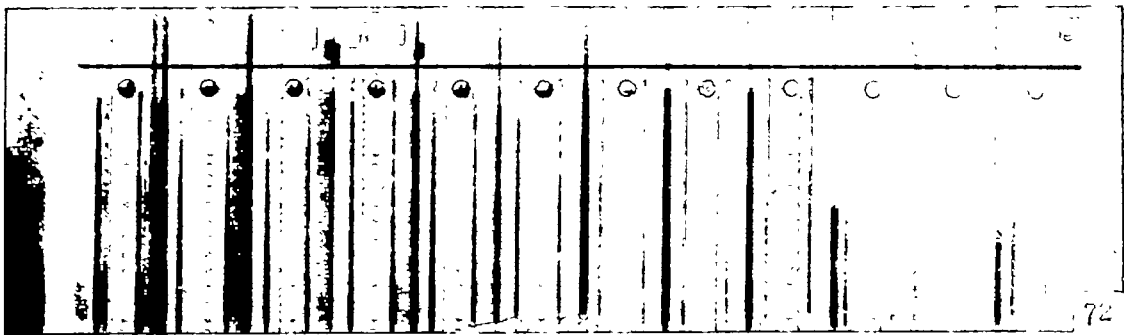
1 2 3 4 5 6 7 8 9 10 11 12 13 14 15 16 17 18 1 2 3 4 5 Ref.
 Probe

(d) $P_o = 1015$ pounds per square inch absolute;
 $T_o = 590^\circ$ R.



1 2 3 4 5 6 7 8 9 10 11 12 13 14 15 16 17 18 1 2 3 4 5 Ref.
 Probe

(e) $P_o = 508$ pounds per square inch absolute;
 $T_o = 590^\circ$ R.

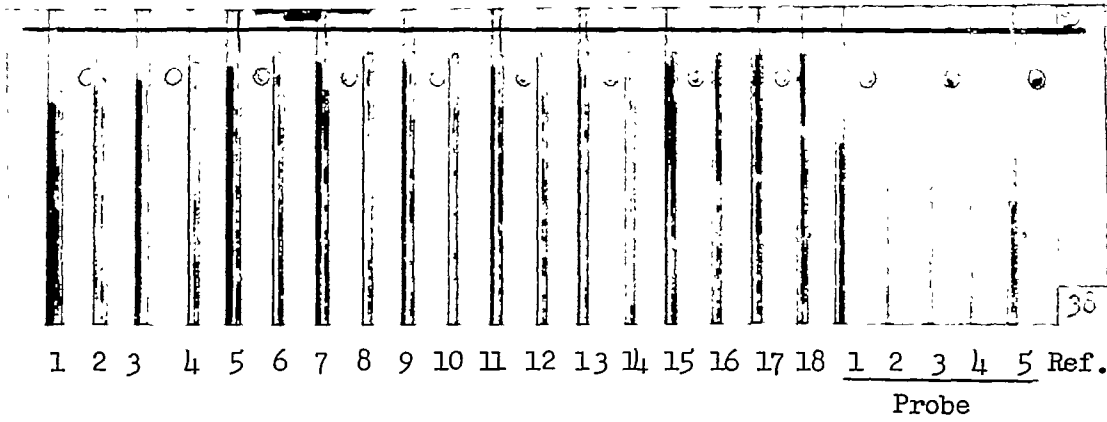


1 2 3 4 5 6 7 8 9 10 11 12 13 14 15 16 17 18 1 2 3 4 5 Ref.
 Probe

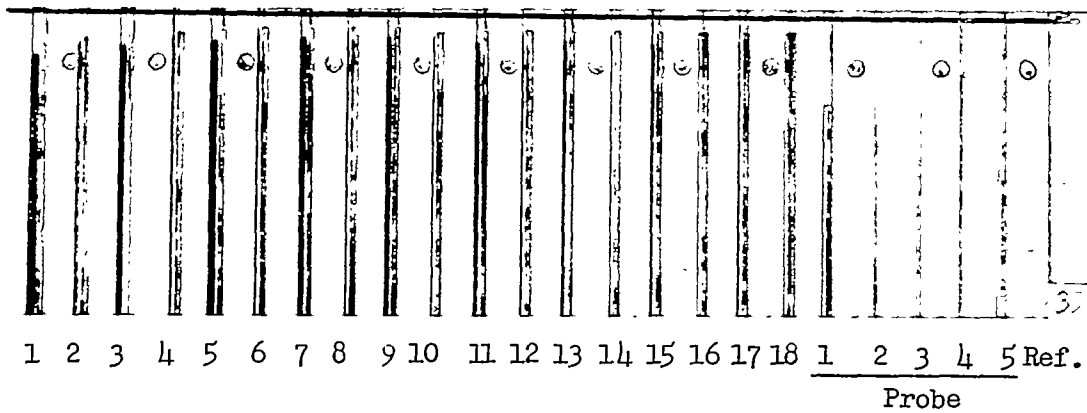
(f) $P_o = 338$ pounds per square inch absolute;
 $T_o = 590^\circ$ R.



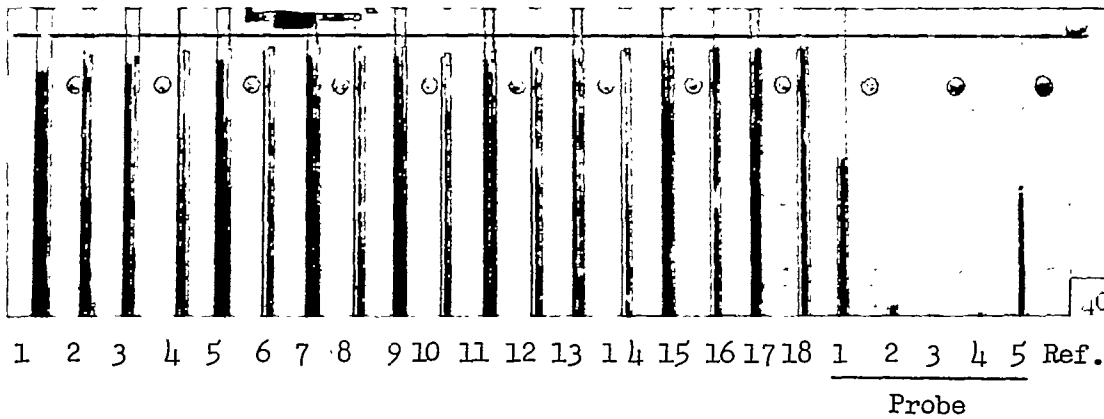
Figure 20.- Continued.



(g) $P_o = 1015$ pounds per square inch absolute;
 $T_o = 977^\circ$ R.



(h) $P_o = 508$ pounds per square inch absolute;
 $T_o = 990^\circ$ R.



(i) $P_o = 338$ pounds per square inch absolute;
 $T_o = 990^\circ$ R.

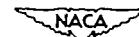
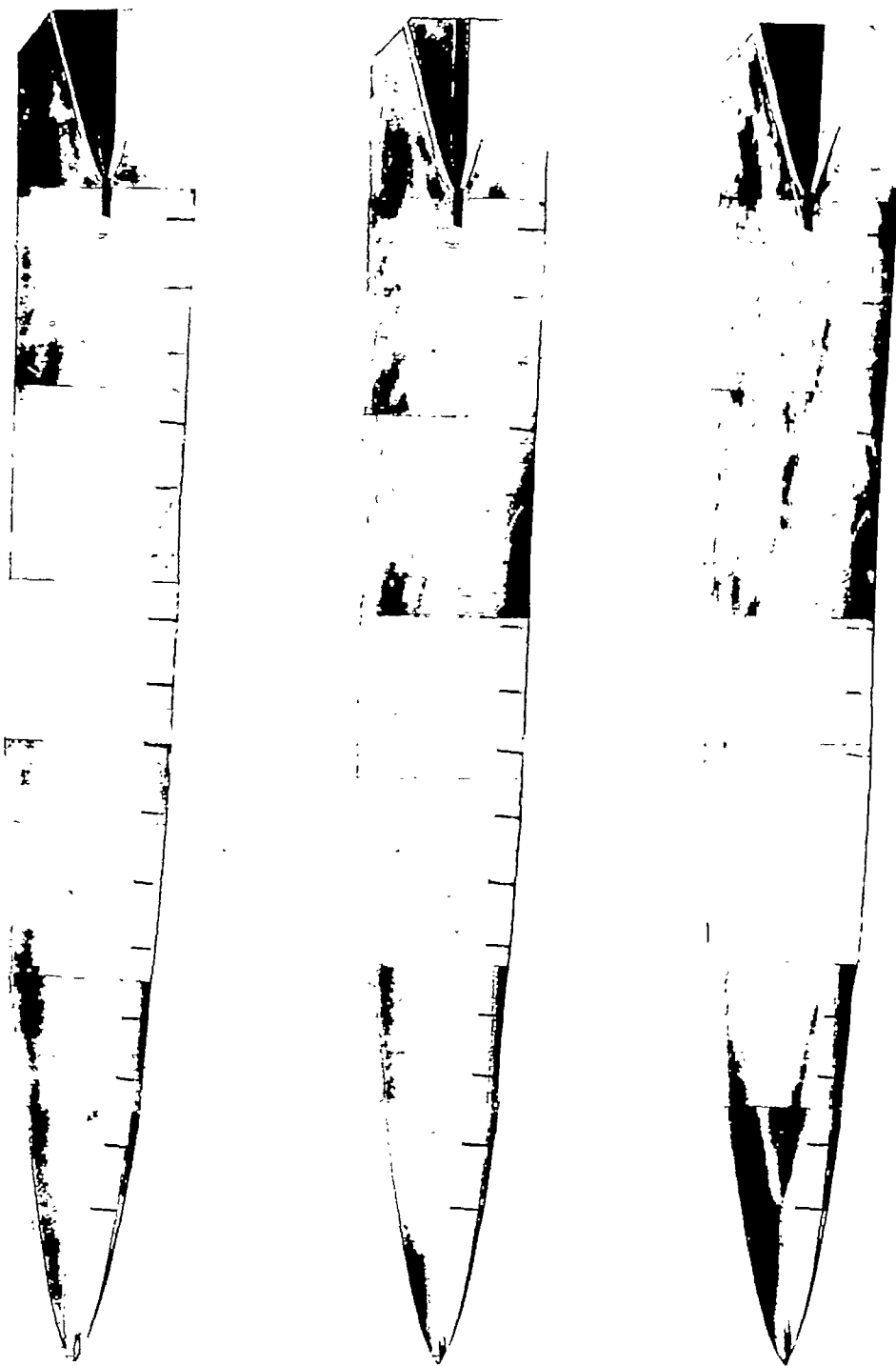


Figure 20.- Concluded.



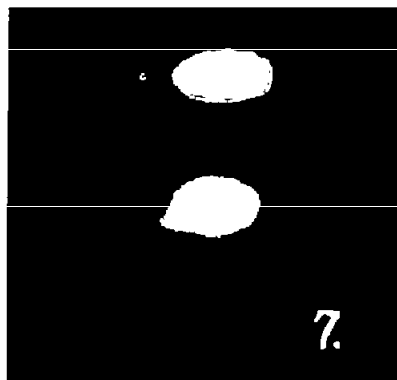
(a) 338 pounds
per square inch
absolute.

(b) 508 pounds
per square inch
absolute.

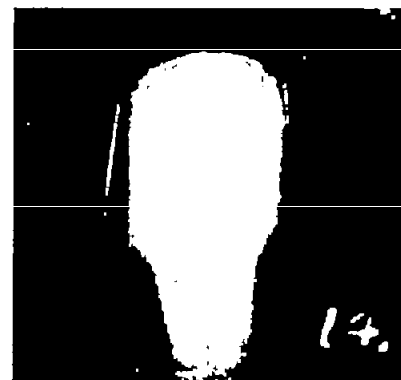
(c) 1015 pounds
per square inch
absolute.



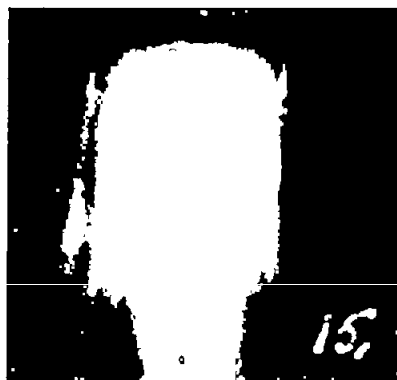
Figure 21.- Schlieren photographs of tunnel at 543° R.



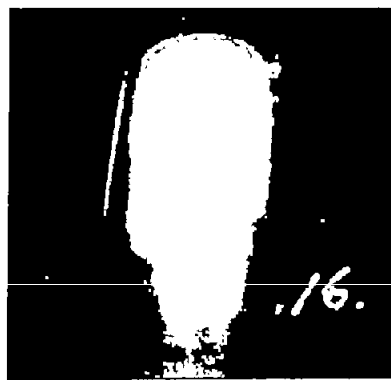
(a) $7\frac{1}{2}$ to $8\frac{1}{2}$ inches from throat.



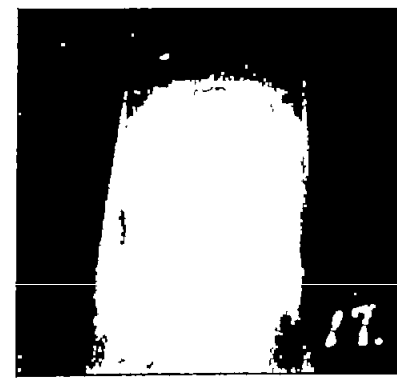
(b) 12 to 14 inches from throat.



(c) 14 to 16 inches from throat.



(d) 16 to 18 inches from throat.



(e) 18 to 20 inches from throat.

Figure 22.- Condensation in test section. All photographs except 7 at f 4.5, 10-second exposure, and $M = 6.5$; photograph 7 at f 4.5 and 10-second exposure with no flow; $P_0 = 1015$ pounds per square inch absolute; $T_0 = 530^\circ$ R.

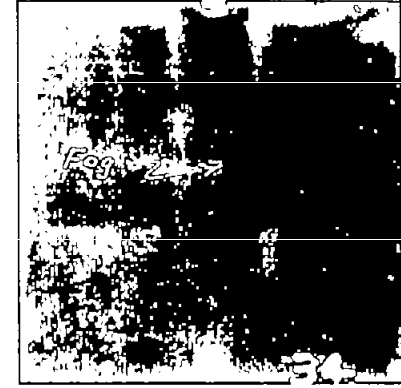




(a) Condensation present;
M = 4.5 to 4.6.



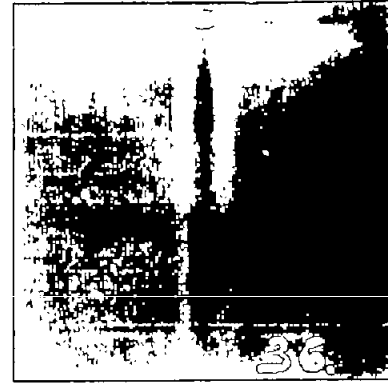
(b) No flow; at same
location as 34.



(c) Beginning of condensation;
M = 4.3 to 4.5.

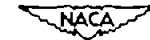


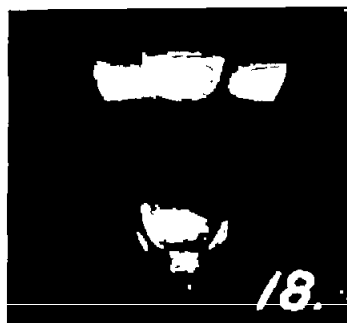
(d) No condensation;
M = 3.9 to 4.3.



(e) No condensation;
M = 3.7 to 3.9.

Figure 23.- Beginning of condensation. All photographs at f 4.5 and 80-second exposure; Mach numbers calculated from area ratios, allowing for boundary-layer build-up; $P_0 = 1015$ pounds per square inch absolute; $T_0 = 530^\circ$ R.





(a) No flow; 1 to 2 inches from throat.



(b) No flow; 1 to 2 inches from throat.



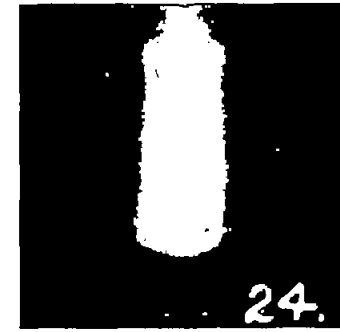
(c) Subsonic; 1 to 2 inches from throat.



(d) $M = 4.9$ to 5.4 ; $P_0 = 1015$ pounds per square inch absolute; 1 to 2 inches from throat.

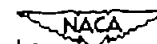


(e) $M = 5.6$ to 6.0 ; $P_0 = 1015$ pounds per square inch absolute; $2\frac{1}{2}$ to $3\frac{1}{2}$ inches from throat.



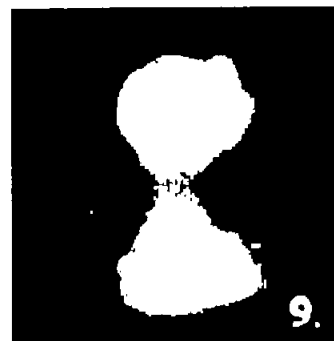
(f) $M = 6.1$ to 6.3 ; $P_0 = 1015$ pounds per square inch absolute; $5\frac{1}{2}$ to $6\frac{1}{2}$ inches from throat.

Figure 24.- Condensation at various Mach numbers. All photographs at f 4.5 and 10-second exposure except 19 and 20 which had 2-minute exposure; $T_0 = 530^\circ$ R.





(a) P_0 , 215 pounds per square inch absolute; 60-second exposure; weight of air, 12.7 pounds.



(b) P_0 , 338 pounds per square inch absolute; 30-second exposure; weight of air, 10 pounds.



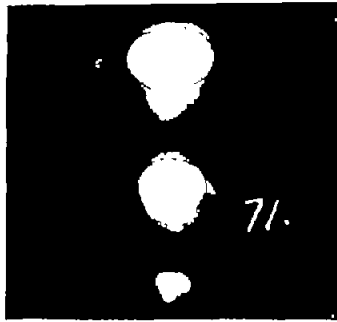
(c) P_0 , 508 pounds per square inch absolute; 20-second exposure; weight of air, 10 pounds.



(d) P_0 , 1015 pounds per square inch absolute; 10-second exposure; weight of air, 10 pounds.

Figure 25.- Condensation at various stagnation pressures. All photographs at f 4.5, $7\frac{1}{2}$ to $8\frac{1}{2}$ inches from throat, and $M = 6.4$ except 8 which is subsonic; $T_0 = 530^\circ$ R.





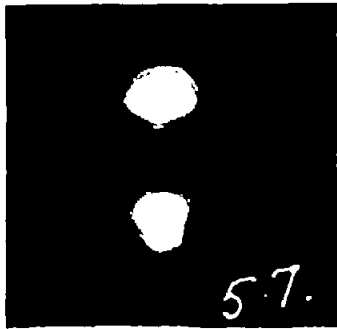
(a) $P_0 = 338$ pounds per square inch absolute; $T_0 = 590^\circ$ R; 16.5-second exposure.



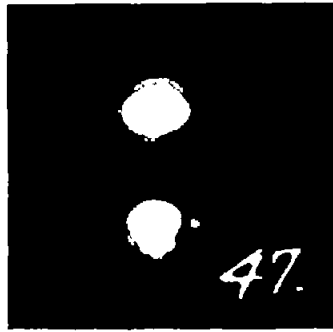
(b) $P_0 = 508$ pounds per square inch absolute; $T_0 = 590^\circ$ R; 11-second exposure.



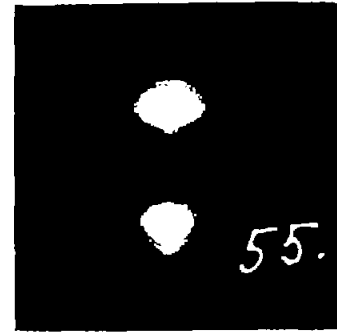
(c) $P_0 = 1015$ pounds per square inch absolute; $T_0 = 590^\circ$ R; 5.5-second exposure.



(d) $P_0 = 338$ pounds per square inch absolute; $T_0 = 980^\circ$ R; 21-second exposure.



(e) $P_0 = 508$ pounds per square inch absolute; $T_0 = 990^\circ$ R; 14-second exposure.



(f) $P_0 = 1015$ pounds per square inch absolute; $T_0 = 1000^\circ$ R; 7-second exposure.

Figure 26.- Condensation at various stagnation pressures and temperatures.

All photographs at f 4, $7\frac{1}{2}$ to $8\frac{1}{2}$ inches from throat, and $M = 6.4$;
weight of air, 5 pounds; Plus X film.



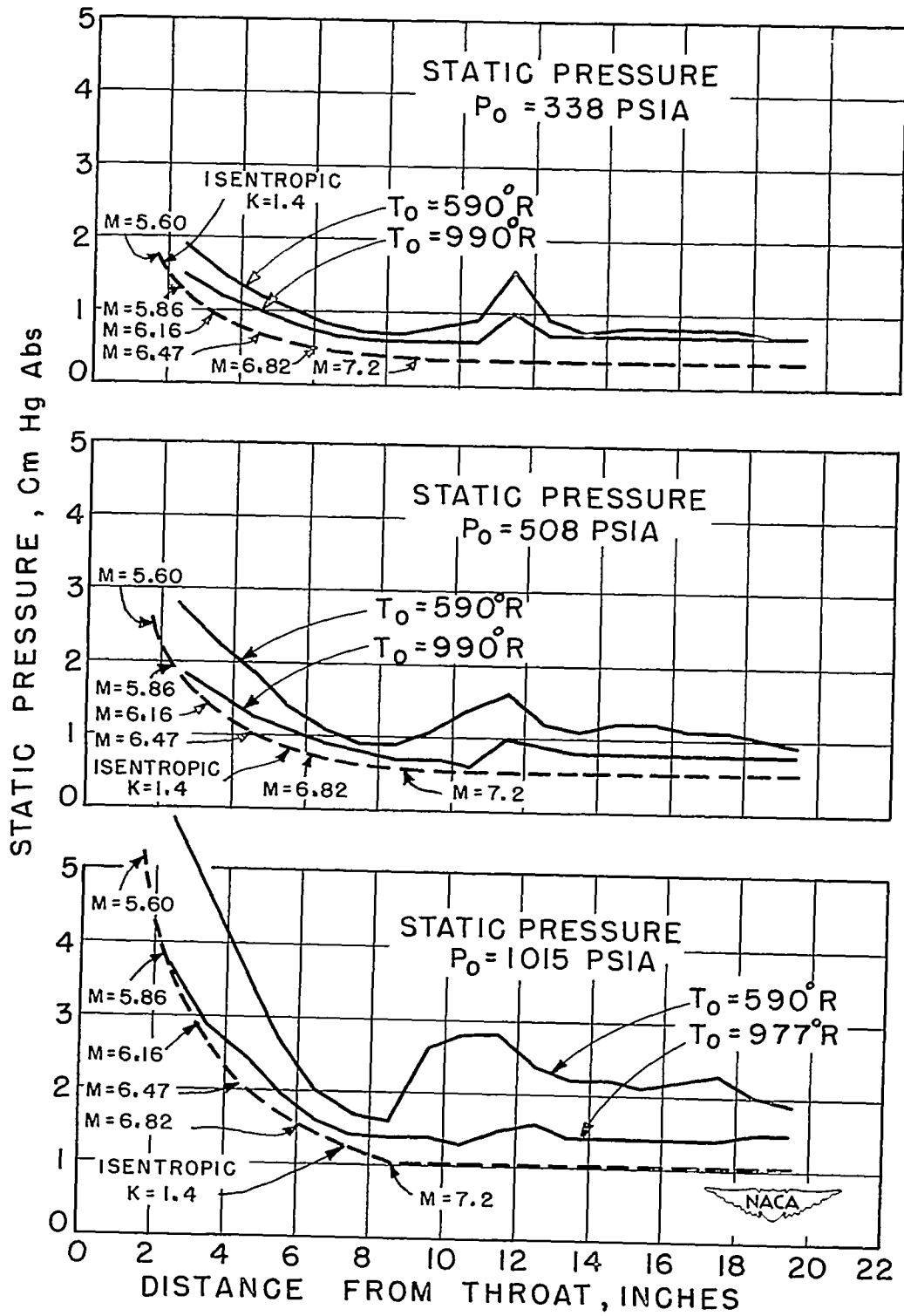
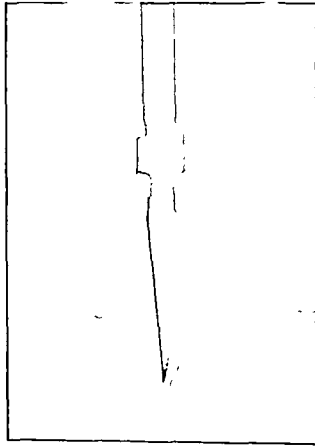
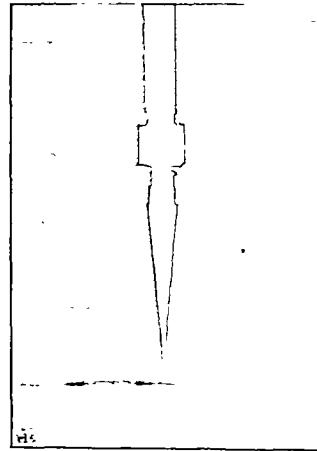


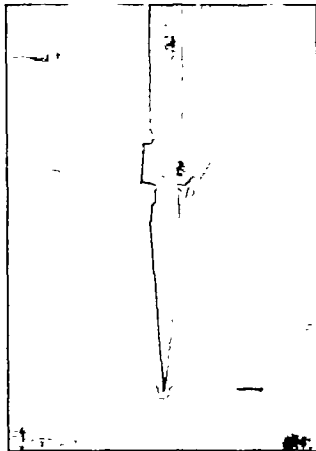
Figure 27.- Static wall pressures at various stagnation pressures and temperatures.



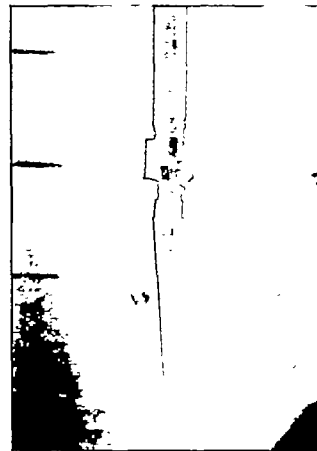
W-3 $\alpha = 15.12^\circ$
 $P_0 = 34.6$ atm., $T_0 = 312^\circ$ K
 $\omega = 5.50^\circ$ } neglecting
 $M = 5.15$ } boundary layer
 $\omega = 6.12^\circ$ } including
 $M = 5.4$ } boundary layer



W-15 $\alpha = 13.48^\circ$
 $P_0 = 34.6$ atm., $T_0 = 413^\circ$ K
 $\omega = 5.50^\circ$ } neglecting
 $M = 6.06$ } boundary layer
 $\omega = 6.32^\circ$ } including
 $M = 6.5$ } boundary layer



W-18 $\alpha = 15.50^\circ$
 $P_0 = 68.6$ atm., $T_0 = 349^\circ$ K
 $\omega = 5.50^\circ$ } neglecting
 $M = 4.93$ } boundary layer
 $\omega = 6.32^\circ$ } including
 $M = 5.3$ } boundary layer



W-9 $\alpha = 13.67^\circ$
 $P_0 = 68.6$ atm., $T_0 = 497^\circ$ K
 $\omega = 5.50^\circ$ } neglecting
 $M = 5.94$ } boundary layer
 $\omega = 6.70^\circ$ } including
 $M = 6.7$ } boundary layer



Figure 28.- Wedge photographs.

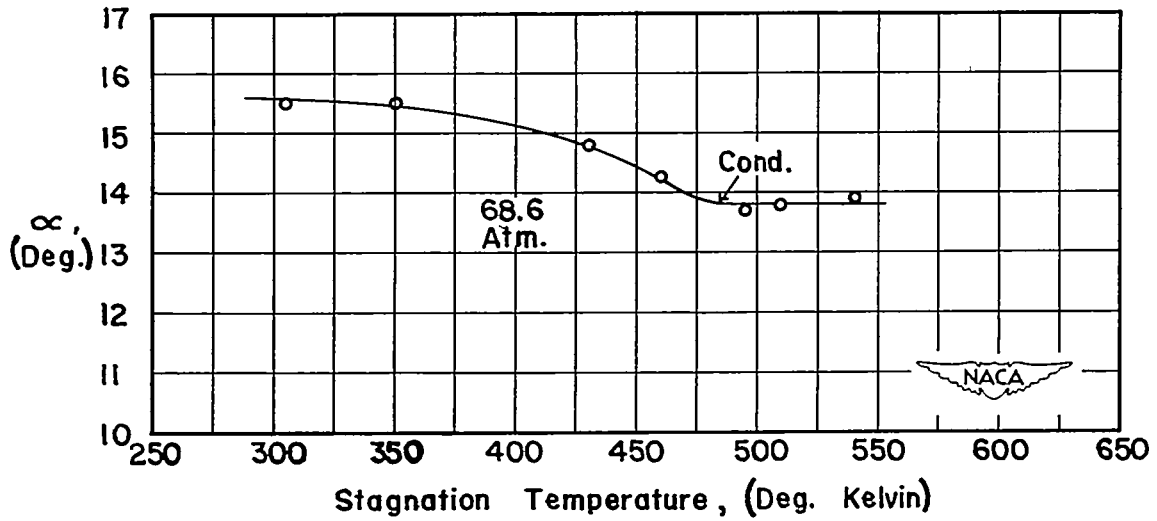
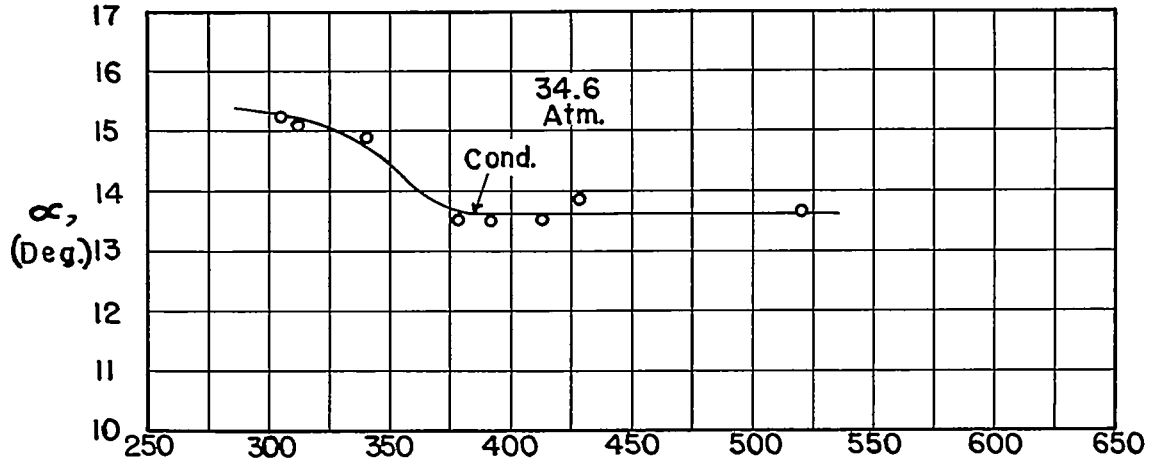
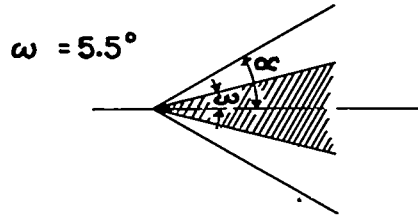


Figure 29.- Effect of stagnation temperature on angle of two-dimensional shock caused by 11° wedge.



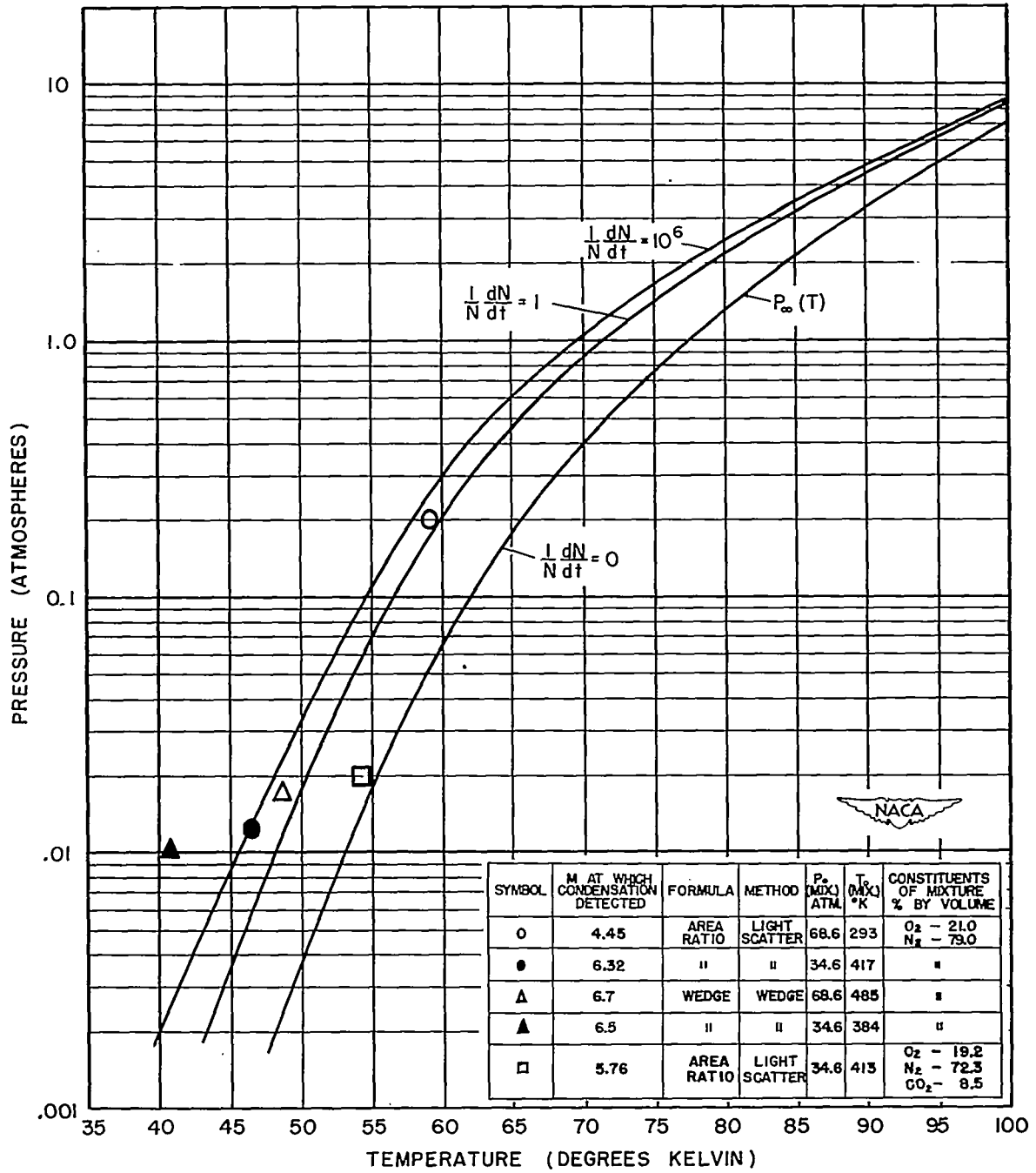


Figure 30.- Nitrogen condensation rates - modified theory with experimental data.

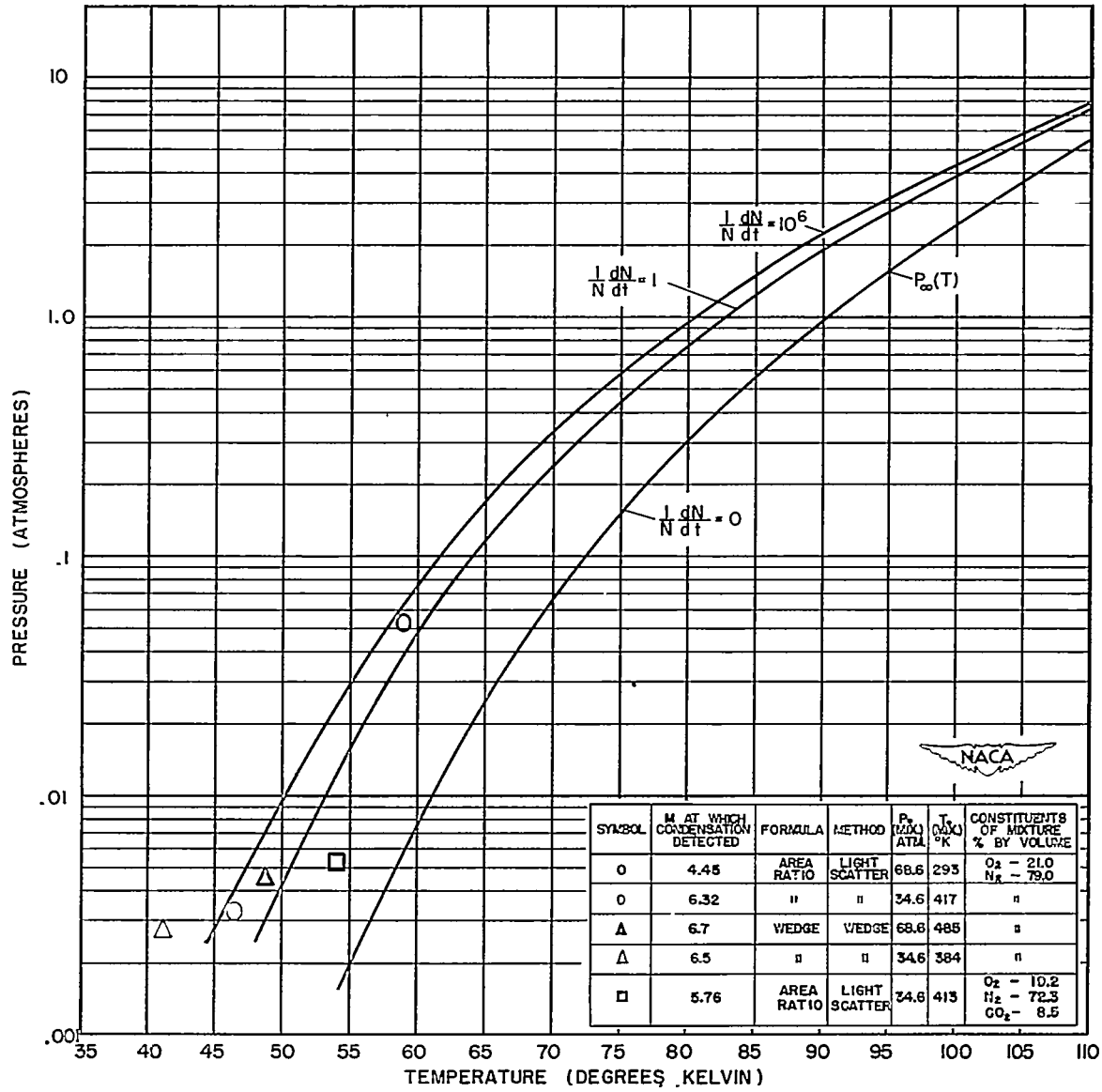


Figure 31.- Oxygen condensation rates - modified theory with experimental data.

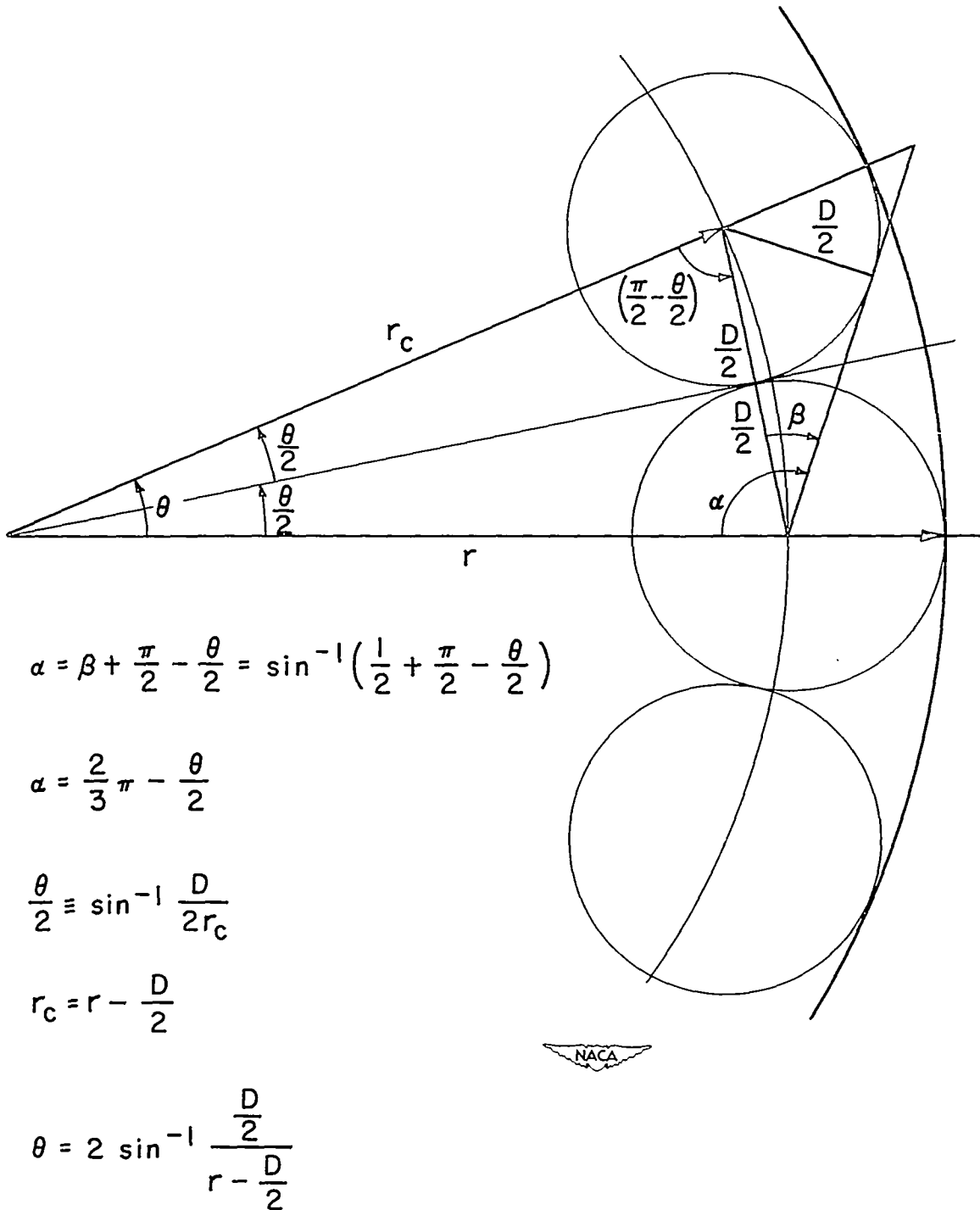


Figure 32.- Geometrical construction for appendix A.